Nuclear Engineering and Technology 54 (2022) 2670–2689

Contents lists available at ScienceDirect

Nuclear Engineering and Technology

journal homepage: www.elsevier.com/locate/net

Original Article

Analysis of several VERA benchmark problems with the photon transport capability of STREAM

Nhan Nguyen Trong Mai, Kyeongwon Kim, Matthieu Lemaire [1], Tung Dong Cao Nguyen, Woonghee Lee, Deokjung Lee*

Department of Nuclear Engineering, Ulsan National Institute of Science and Technology, 50 UNIST-gil, Ulsan, 44919, Republic of Korea

ARTICLE INFO

Article history:
Received 10 November 2021
Received in revised form
19 January 2022
Accepted 5 February 2022
Available online 9 February 2022

Keywords:
Photon transport
Photon KERMA
Multigroup photon library
Fixed source solver

ABSTRACT

STREAM - a lattice transport calculation code with method of characteristics for the purpose of light water reactor analysis - has been developed by the Computational Reactor Physics and Experiment laboratory (CORE) of the Ulsan National Institute of Science and Technology (UNIST). Recently, efforts have been taken to develop a photon module in STREAM to assess photon heating and the influence of gamma photon transport on power distributions, as only neutron transport was considered in previous STREAM versions. A multi-group photon library is produced for STREAM based on the ENDF/B-VII.1 library with the use of the library-processing code NJOY. The developed photon solver for the computation of 2D and 3D distributions of photon flux and energy deposition is based on the method of characteristics like the neutron solver. The photon library and photon module produced and implemented for STREAM are verified on VERA pin and assembly problems by comparison with the Monte Carlo code MCS – also developed at UNIST. A short analysis of the impact of photon transport during depletion and thermal hydraulics feedback is presented for a 2D core also from the VERA benchmark.

1. Introduction

The energy released in a nuclear reactor is mostly recoverable from the kinetic energy of fission fragments, photons from fission and neutron capture, beta from decay of fission products and neutron scattering [1]. Fission fragments and decay betas give off their energy within a relatively short range and can be treated as locally deposited in the fuel [2]. Neutrons and photons have longer mean-free-paths and can move to other regions and deposit their energies further away. The recoverable energy from fission, however, is historically computed in deterministic codes by the multiplication of the fission rate with the energy release per fission, a.k.a. Kappa value and the explicit photon transport is not performed to reduce the computational burden. In that case, the photon energies are assumed to be locally deposited and are either incorporated into the Kappa value or smeared throughout the problem [2–5]. The great gradient of photon flux distribution in core geometries featuring strong gamma emitters or leakage can deteriorate the accuracy of these assumption since gammas are unlikely to be uniformly distributed in such problems and will most likely not deposit their energies at birth places but elsewhere further away. Thus, the accurate calculation of energy deposition maps in those problems requires explicit photon transport.

The introduction of explicit photon transport into calculation chains has become a common way of addressing those issues [6,7]. The most important purpose of performing photon transport is to compute the photon heating, often approximated as photon KERMA (Kinetic Energy Release per MAss [8]), from calculated photon flux. A photon transport option has been available in several lattice codes such as APOLLO2, HELIOS and CASMO for two-dimensional (2D) calculations [9–11]. Whole core photon transport has also been deployed in the deterministic codes WIMS

* Corresponding author. School of Mechanical, Aerospace and Nuclear Engineering, Ulsan National Institute of Science and Technology, 50 UNIST-gil, Eonyang-eup, Ulju-gun, Ulsan, 44919, Republic of Korea.
E-mail addresses: mainhan@unist.ac.kr (N.N.T. Mai), kyeongwon@unist.ac.kr (K. Kim), matthieu.lemaire@cea.fr (M. Lemaire), tungnguyen@unist.ac.kr (T.D.C. Nguyen), dldndgml0310@unist.ac.kr (W. Lee), deokjung@unist.ac.kr (D. Lee).
[1] Matthieu Lemaire was affiliated with Department of Nuclear Engineering, Ulsan National Institute of Science and Technology, 50 UNIST-gil, Ulsan 44919, Republic of Korea. He is now affiliated with Université Paris-Saclay, CEA, Service d'Études des Réacteurs et de Mathématiques Appliquées, 91191, Gif-sur-Yvette, France.

https://doi.org/10.1016/j.net.2022.02.004

(2017), nTRACER (2020) and MPACT (2020) [12–14] but the literature is limited to small problems without thermal-hydraulics feedback and depletion. For three-dimensional (3D) whole-core calculations with thermal hydraulics (TH) feedback, the explicit calculation of the photon KERMA is valuable to determine the fraction of fission energy directly deposited in the moderator and cladding. By contrast, the Kappa value method only provides the energy deposition in the fuel regions while the heating in other materials such as cladding is disregarded and the heating in the moderator is usually pre-determined by user preferences. In addition, explicit photon transport is able to capture better the complexities of 3D geometries (with material or structure variations in both radial and axial directions) than the assumptions of local deposition or uniform smearing of photon energies. The accurate calculation of gamma heating with quantified uncertainties in non-fuel zone in Gen III + or Gen IV reactors is also an important industrial stake for performance and safety reasons [15]. The heating in a stainless-steel reflector, for example, is dominated by gammas and must be calculated precisely to prevent the contact/damage to the peripheral core fuel assemblies induced by excessive thermal expansion of the reflector.

To better predict photon KERMA/power map distributions and improve TH calculations for high-fidelity analysis of reactor problems, a photon transport module has been implemented in the STREAM code developed by the Computational Reactor Physics and Experiment Laboratory (CORE) at the Ulsan National Institute Science and Technology (UNIST). STREAM – a deterministic neutron-transport analysis code– uses the method of characteristics to solve the multi-group neutron transport equation for the analysis of 2D or 3D cores with high accuracy [16]. Notable features implemented in STREAM include pin-based pointwise energy slowing-down method for resonance treatment [17], automatic thermal expansion, few-group constant generation for nodal codes [18], sub-channel thermal-hydraulic calculation, and source term calculation [19]. The development efforts for the photon module in STREAM include the generation of a multi-group photon library based on the Evaluated Nuclear Data File (ENDF) B-VII.1 library [20] with the use of NJOY code [21] and the adaptation of the solver already present for the neutron transport calculation to obtain distributions of photon flux and energy deposition.

The plan of the article is as follows. First, the STREAM multi-group photon library and the photon flux solver are described. Then, the verification of the generated photon library and of the photon flux solver is conducted for a set of problems available with in-depth details from the VERA benchmark [22]. The 2D benchmarks VERA 1B, VERA 2B, VERA 2P and the 3D benchmark VERA 4 are selected for their representativity of typical Light Water Reactor (LWR) configurations, namely the simple fuel pin, the 2D fuel lattices without and with poisons and the 3D assembly array with control rods. The verification is conducted on the different calculation steps, from the derivation of the gamma source from the neutron flux and the gamma production cross sections, to the application of this gamma source and of the photo-atomic cross sections in the photon flux solver for the transport calculation, until the computation of the photon KERMA from the photon flux solution. Thus, the neutron flux, gamma production, photon flux and photon energy deposition throughout depletion in the different material regions (fuel, cladding and water) of the selected VERA problems are computed by STREAM and compared against the results obtained from the Monte Carlo (MC) code MCS [23] (also developed at UNIST in the CORE laboratory). Afterwards, a short analysis with STREAM for the impact of the explicit photon transport on a depletion calculation with TH feedback is considered for a 2D VERA core problem. Finally, conclusions and perspectives for future work are drawn out.

2. Photon library and photon fixed source solver

2.1. Photon library

A library for photon transport must include the gamma production cross sections (to compute the gamma sources from neutron interactions) and the photo-atomic cross sections (to compute the actual photon transport from gamma sources). The GROUPR module in NJOY generates prompt gamma production matrices while the GAMINR module calculates multi-group photo-atomic cross sections and group to group photon scattering matrices. The generation of the multi-group photon library for STREAM is detailed in reference [24]. Currently, the photon library in STREAM employs 72 neutron energy groups for the gamma production cross sections and 18 photon energy groups ranging from 1 keV to 10 MeV for the photo-atomic cross sections. The energy boundaries for neutron and photon calculation in STREAM are provided in the supplement data.

The multi-group photon library for STREAM includes the gamma-production cross-section matrices of 425 nuclei processed at seven different temperatures (293.6 K, 600 K, 900 K, 1200 K, 1500 K, 1800K, 2100 K). The generated cross-section matrices from GROUPR include:

- the nonelastic production matrix (MF16, MT3);
- the inelastic production matrix (MF16, MT4 and MT50-91);
- the fission production matrix (MF16, MT18–21 and MT38);
- the capture production matrix (MF16, MT102);
- a “other production” matrix which represents all the other, rarer neutron reactions that can produce gamma photons, such as *(n, 2n)* and *(n, pα)*.

The total matrix for prompt gamma ($p\gamma$) production is simply calculated as the sum of the partial matrices as in Equation (1) where the indices of the neutron and photon energy group are denoted as n and g, respectively.

$$\sigma^{p\gamma}_{n\to g} = \sigma^{capture}_{n\to g} + \sigma^{fission}_{n\to g} + \sigma^{inelastic}_{n\to g} + \sigma^{nonelastic}_{n\to g} + \sigma^{others}_{n\to g} \quad (1)$$

The photo-atomic cross sections and matrices are available for 100 elements (Z = 1 to 100). The generated photo-atomic data from GAMINR includes:

- the total (*tot*) cross section (MF23, MT501);
- the coherent scattering cross section (MF23, MT502);
- the incoherent scattering cross section (MF23, MT504);
- the pair production cross section (MF23, MT516);
- the photoelectric absorption cross section (MF23, MT522);
- the heat production cross section (MF23, MT525);
- the coherent (*coh*) scattering matrix (MF26, MT502);
- the incoherent (*incoh*) scattering matrix (MF26, MT504);
- the pair production (*pp*) scattering matrix (MF26, MT516).

The pair production creates an electron-positron pair and the subsequent annihilation of the positron generates two gammas having energy of 0.511 MeV each. Thus, the pair production is simply treated as $(\gamma, 2\gamma')$ scattering and incorporated into the scattering matrix $\sigma^{\gamma}_{s,g\to g'}$ via Equation (2) where the number 0 index is the Legendre scattering order:

$$\sigma^{\gamma}_{s,g\to g'} = \sigma^{\gamma}_{coh,0,g\to g'} + \sigma^{\gamma}_{incoh,0,g\to g'} + \sigma^{\gamma}_{pp,0,g\to g'} \quad (2)$$

The multi-group photon transport equation is solved with a MOC flux solver assuming only isotropic scattering. The outflow transport correction [25] is applied to the self-scattering term

$\sigma^{\gamma}_{s,g\to g}$ in the scattering matrix and the total cross section σ^{γ}_{tot} is adjusted accordingly as in Equations (3) and (4) where the number 1 index inside the summation is the Legendre scattering order.

$$\sigma^{\gamma}_{s,g\to g} = \sigma^{\gamma}_{s,g\to g} - \sum_{g'=1}^{18} \sigma^{\gamma}_{incoh,1,g\to g'} \tag{3}$$

$$\sigma^{\gamma}_{tr,g} = \sigma^{\gamma}_{tot,g} - \sum_{g'=1}^{18} \sigma^{\gamma}_{incoh,1,g\to g'} \tag{4}$$

In other codes such as SERPENT [26], OpenMC [27] and MPACT [28], the delayed fission gamma can be accounted for by means of a weighting factor $f = \frac{EGD}{EGP}$ applied to the prompt fission gamma [14,29,30] where EGP and EGD are the prompt and delayed gamma energy release per fission from the ENDF MT458 data [31]. This approach for delayed fission gamma is currently applied in STREAM where the delayed fission gamma production cross section matrix $\sigma^{d\gamma}_{n\to g}$ is derived simply by multiplying the prompt fission gamma production cross section matrix $\sigma^{fission}_{n\to g}$ defined in Equation (1) with f:

$$\sigma^{d\gamma}_{n\to g} = f\cdot\sigma^{fission}_{n\to g} \tag{5}$$

The photon heat production cross section is calculated by GAMINR in NJOY with the assumption that the fluorescence photons deposit their energies locally [32]. The basis of this assumption lies in the low energy of fluorescence photons, below 150 keV. The photon KERMA (K^{γ}) is then simply obtained by the convolution of the photon flux from the fixed source solver with this heat production cross section as shown in Equation (6) where ϕ_g and $\Sigma^{\gamma}_{K,g}$ is the flux and heat production macroscopic cross section of photon in group g, respectively.

$$K^{\gamma} = \sum_{g=1}^{18} \phi^{\gamma}_{g}\Sigma^{\gamma}_{K,g} \tag{6}$$

It is worth noting a multigroup spectrum is required as a weighting function during the generation of the multigroup cross section [21]. Instead of using NJOY default simplified neutron and photon spectra, a spectrum of neutron flux (hundred thousand groups) and a spectrum of photon flux (ten thousand groups), representative of a typical LWR pin, were calculated with the Monte Carlo code MCS with significant number of histories to reduce the uncertainty to less than 1% for most of the energy bins and then used as weighting functions in NJOY to enhance the accuracy of the photon multigroup cross sections.

During the actual transport of photons, secondary photons are created by means of atomic relaxation and Bremsstrahlung [33]. During Compton scattering events, a Doppler effect can also occur due to the momentum of the shell electron colliding with the incoming photon [33]. Unfortunately, these photon physics are not yet available in STREAM and the photon flux derived from STREAM with the current photon library set does not contain the contribution from such secondary photons. The energy deposition from those photons created by atomic relaxation and Bremsstrahlung are nevertheless included in the KERMA calculation by means of heat production cross sections that consistently assumes that those photons always deposit their energies locally at birth.

2.2. Photon fixed-source solver

The photon transport equation is shown in Equation (7) where: ψ^{γ}_{g} is the angular photon flux, $\Sigma^{\gamma}_{tr,g}$ is the macroscopic transport-corrected total cross section, $Q^{N\gamma}_{g}$ is the neutron-induced gamma source and $\Sigma^{\gamma}_{s,g'\to g}$ is the macroscopic transport-corrected scattering cross section.

$$\widehat{\Omega}\cdot\nabla\psi^{\gamma}_{g} + \Sigma^{\gamma}_{tr,g}\psi^{\gamma}_{g} = Q^{N\gamma}_{g} + \sum_{g'=1}^{18}\Sigma^{\gamma}_{s,g'\to g}\phi^{\gamma}_{g'} \tag{7}$$

$Q^{N\gamma}_{g}$ is obtained by the convolution of the neutron flux with the gamma production cross section as in Equation (8)

$$Q^{N\gamma}_{g} = Q^{p\gamma}_{g} + Q^{d\gamma}_{g} = \sum_{n=1}^{72}\phi^{N}_{n}\Sigma^{p\gamma}_{n\to g} + \sum_{n=1}^{72}\phi^{N}_{n}\Sigma^{d\gamma}_{n\to g} \tag{8}$$

where: $Q^{p\gamma}_{g}$ is the prompt gamma source and $Q^{d\gamma}_{g}$ is the delayed fission gamma source, ϕ^{N}_{n} is the neutron flux in group n, $\Sigma^{p\gamma}_{n\to g}$ and $\Sigma^{d\gamma}_{n\to g}$ are the prompt gamma production cross section and delayed fission gamma production cross section from neutron group n to photon group g, respectively.

The photon flux calculation is performed as a fixed source problem. Equation (7) has a similar form to the neutron transport equation, making it possible to adopt several parts of the existing neutron flux solver for the photon flux solver. The flux solver of STREAM is described in detail in Ref. [34]. The photon KERMA is obtained from Equation (5) once the photon flux has converged.

3. Verification of photon transport calculation against MCS

STREAM employs the method of characteristics to solve the transport equation in the form of multigroup calculation where approximations are introduced (e.g., multigroup cross section generation with resonance treatment, geometry discretization). Monte Carlo codes, however, simulate the particle transport with detailed physics processes and interactions in exact geometries, giving the utmost accuracy. To best verify the photon transport capability in STREAM, comparison with a MC code is conducted and the MCS code is selected for this purpose.

MCS – a Monte Carlo-based 3D continuous-energy neutron- and photon-physics code for particle transport– has been developed at UNIST since 2013 [23]. The neutron transport and collision kernel of MCS is verified and validated against several benchmarks, including benchmarks from the International Criticality Safety Benchmark Experimental Problem (ICSBEP) database [35], the Benchmark for Evaluation and Validation of Reactor Simulations (BEAVRS) [36], and the Very High Temperature Reactor (VHTR) [37]. The photon transport kernel is verified [38] against MC codes MCNP6.1 [39] and SERPENT2.1.29 [27]. The coupled neutron-photon transport mode in MCS is available in both criticality and fixed source mode and has been validated against benchmarks from the Shielding Integral Benchmark Archive and Database (SINBAD) [40,41].

The quantities verified in the following sections are the neutron flux, the gamma production, the photon flux, and the photon KERMA. Those quantities are calculated with both STREAM and MCS in different material regions during the criticality calculation in coupled neutron-photon transport mode. Detailed comparison between STREAM and MCS is presented for the VERA 1B case while only photon KERMA comparison is presented for the 2D lattice and the 3D case. To ensure consistent comparisons, a scaling factor C is applied to all the STREAM results presented in this paper so that the STREAM results are normalized in the same way as the MCS results, that is, normalized per one neutron source. The scaling factor C is

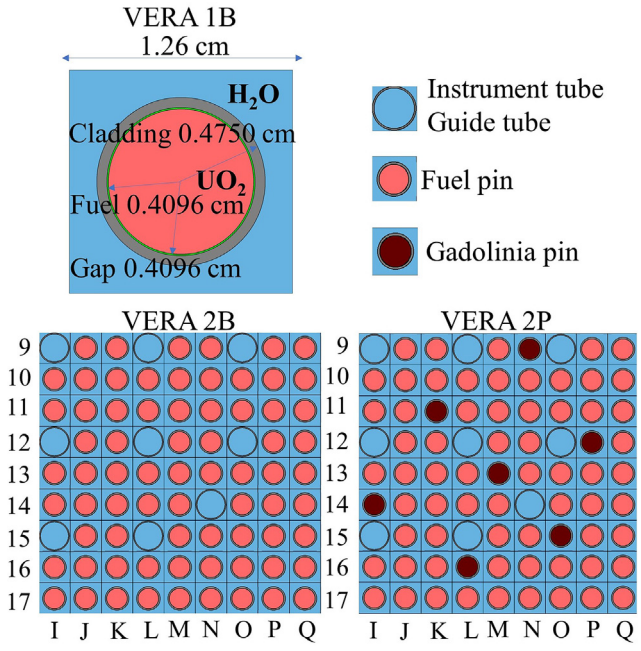

Fig. 1. VERA 1B pin cell, VERA 2B and VERA 2P lattice (quarter geometry).

Table 1
k_{eff} of VERA 1B at BOC, MOC and EOC from STREAM and MCS.

Burnup	MCS	STREAM	Difference (pcm)
BOC	1.18138 ± 0.00024	1.18134	−4 ± 24
MOC	0.90884 ± 0.00018	0.91031	147 ± 18
EOC	0.79867 ± 0.00019	0.80055	188 ± 19

defined as the ratio of the total fission source between MCS and STREAM as shown in Equation (9).

$$C = \frac{MCS's\ total\ fission\ source}{STREAM's\ total\ fission\ source} \tag{9}$$

MCS results are used as references in the comparison with STREAM and the relative difference (*Rel. Diff.*) is defined as in Equation (10).

$$Rel.\ Diff. = \left(\frac{STREAM's\ results}{MCS's\ results} - 1\right) \times 100\% \tag{10}$$

All the calculations in this paper are conducted with the ENDF/B-VII.1 library. For the three investigated burnup steps, namely at 0 MWd/kg (beginning of cycle BOC), 30 MWd/kg (middle of cycle MOC) and 60 MWd/kg (end of cycle EOC), consistency is enforced between the input material compositions of STREAM and MCS by first generating the depleted number densities with the depletion module of MCS and then using those depleted compositions in STREAM's calculations. An input power density of 40 W/gHM (watts per gram of heavy metal) [42] is used in the MCS depletion calculation. The configurations of the VERA 1B, VERA 2B and VERA 2P lattices are shown in Fig. 1. Only prompt gammas are considered in the verification because the delayed fission gamma production is not available in MC codes like MCNP or MCS and this delayed source in STREAM is simply scaled from the prompt fission gamma source.

3.1. VERA 1B: 2D pin cell

The VERA 1B pin cell initially has 3.1 wt percent (w/o) enriched uranium oxide fuel and a pitch of 1.26 cm. Both fuel and moderator temperature are set at 600 K. Results of k_{eff} (effective neutron multiplication factors) are shown in Table 1, in which increased differences are observed with increasing burnups. The neutron flux and the gamma production in the fuel region of VERA 1B pin are illustrated in Fig. 2. A reasonable agreement is observed for the gamma production with small differences increasing with the burnup. The resonance treatment of STREAM in the multigroup neutron cross sections for the additional nuclides showing up at

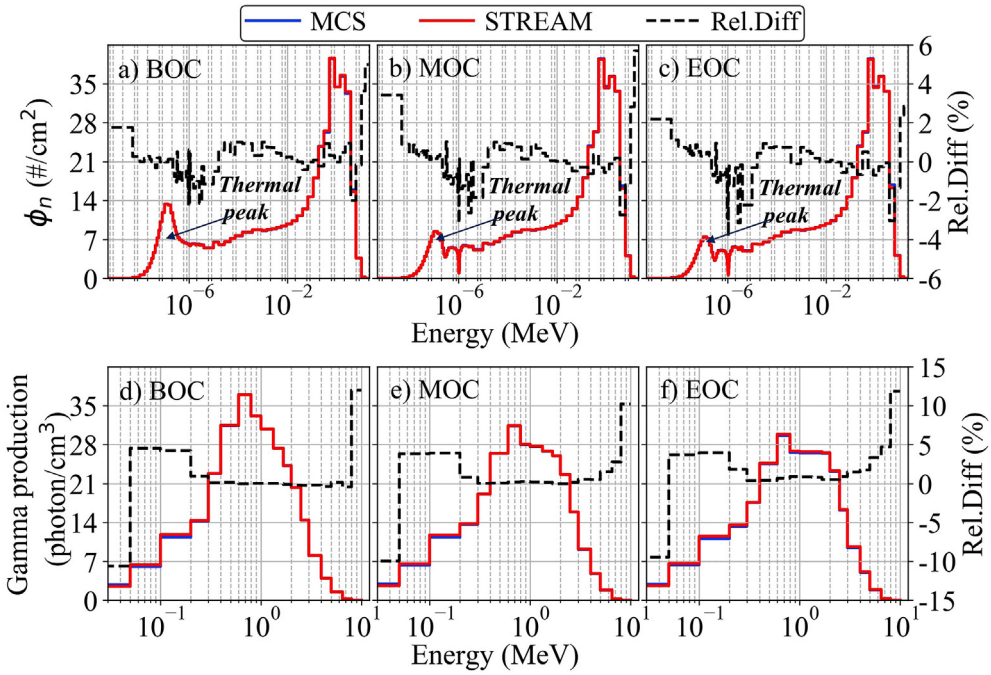

Fig. 2. Neutron flux and gamma production in fuel region of VERA 1B (normalized by one neutron source).

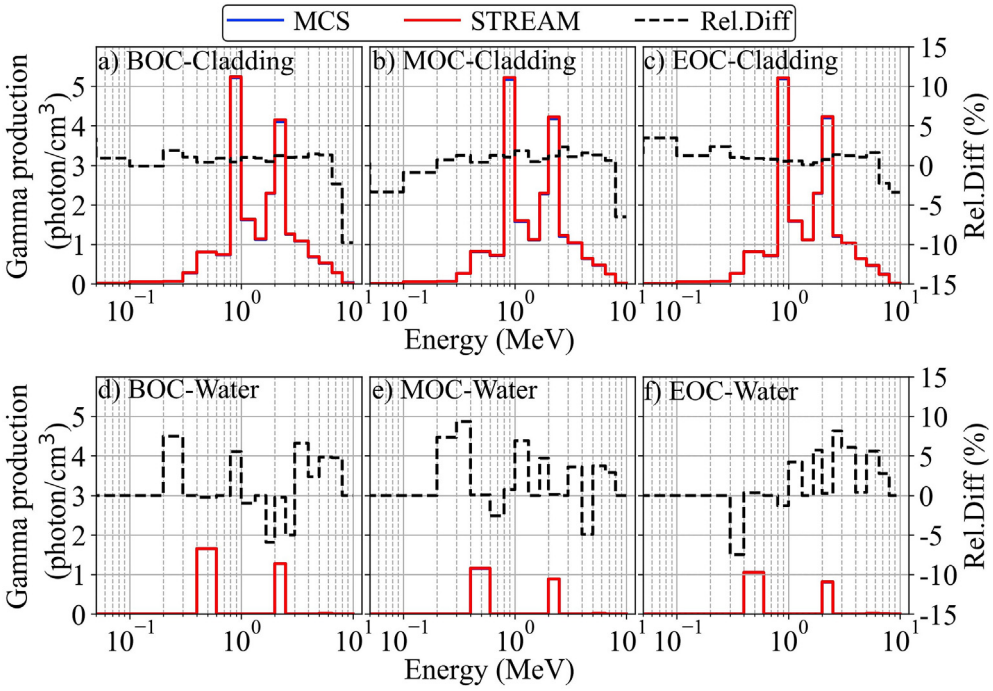

Fig. 3. Gamma production in cladding and water regions of VERA 1B (normalized by one neutron source).

later burnups introduces an overestimation by a few percent of the thermal neutron flux of STREAM compared to MCS (see Fig. 2b and c), and this overestimation in the thermal neutron range leads to the observed differences in the gamma production in fuel and in the k_{eff}.

The gamma production in the cladding and water region are shown in Fig. 3. The shape of the gamma source in the cladding remains rather unchanged during depletion while the magnitude of the two peaks in the gamma source of water, corresponding to the gammas emitted from the thermal neutron capture of ^{10}B and ^{1}H (0.477 keV and 2.223 MeV [43], respectively), decreases due to the reduction in the magnitude of the thermal neutron peak. It

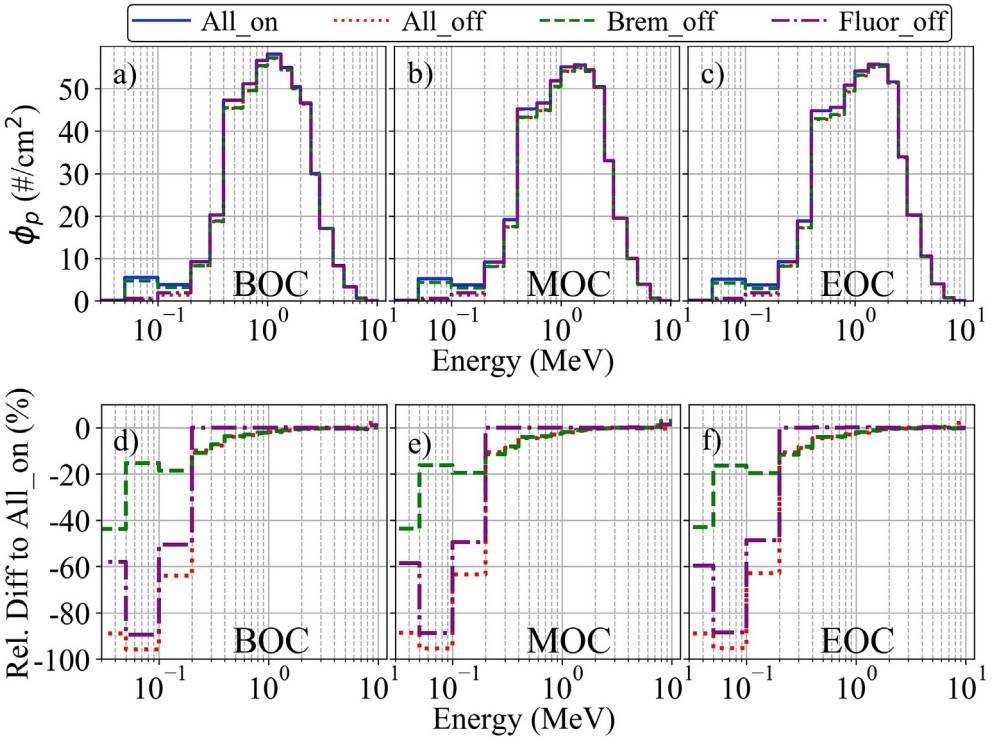

Fig. 4. MCS photon flux in the fuel region of VERA 1B (normalized by one neutron source).

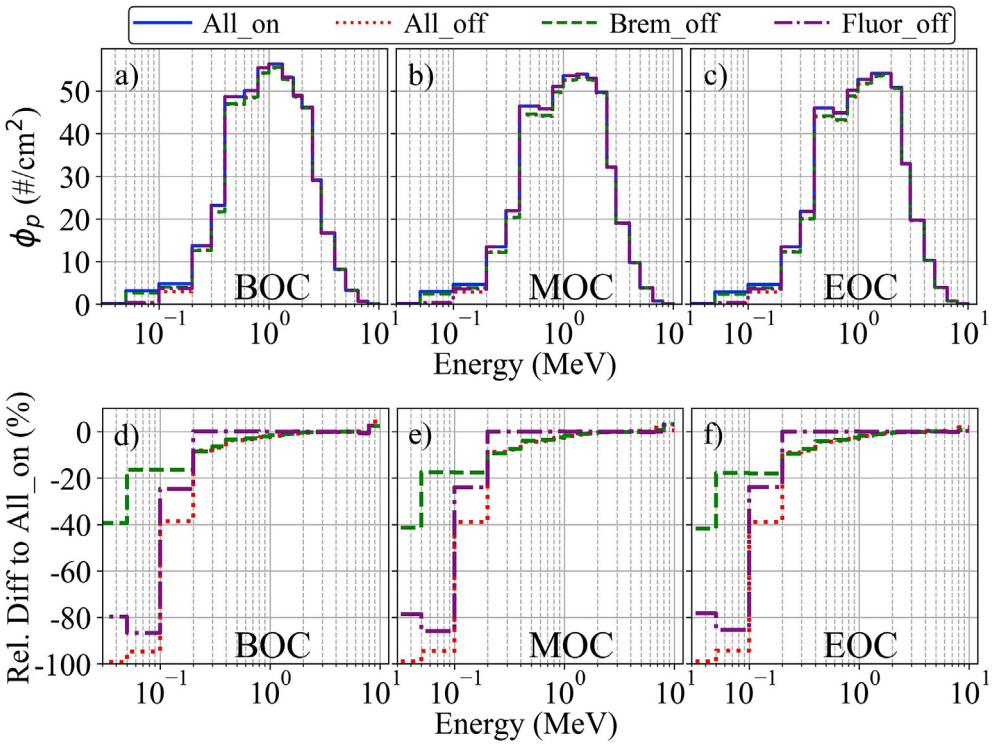

Fig. 5. MCS photon flux in the cladding region of VERA 1B (normalized by one neutron source).

should be noted that most gammas are generated by fission in the fuel and the gamma sources in the cladding and water have much lower intensities.

The impact of atomic relaxation, Bremsstrahlung and Doppler broadening of Compton scattering (which are not implemented in STREAM) on the photon flux and KERMA of the VERA 1B pin are assessed with the Monte Carlo code MCS, in which those specific physics can be turned on or off by the user. The phrase "*All on*" in

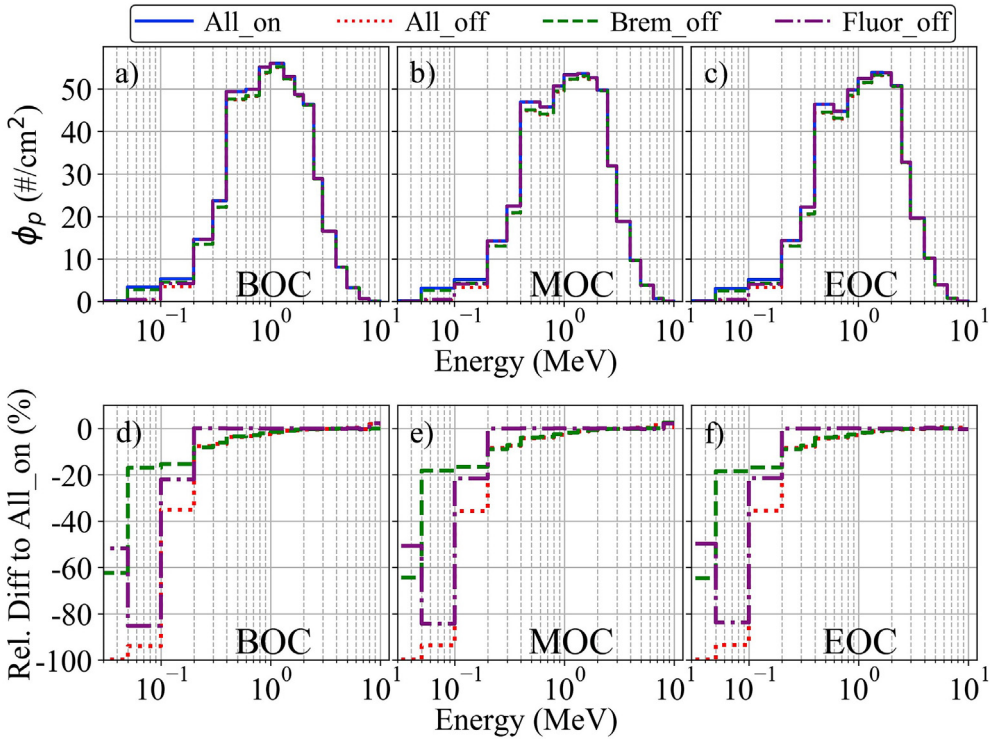

Fig. 6. MCS photon flux in the water region of VERA 1B (normalized by one neutron source).

the paper represents calculations in which atomic relaxation and Bremsstrahlung are turned on in MCS, "*All off*" calculations where they are turned off, "*Relaxation off*" or "*Bremsstrahlung off*" indicates that only atomic relaxation or Bremsstrahlung is turned off respectively. The photon flux obtained by MCS with the different photon physics options throughout depletion are compared in Fig. 4 for fuel, Fig. 5 for cladding and Fig. 6 for water. The values of photon KERMA obtained by MCS throughout depletion with the different photon physics options are presented in Table 2. The statistical errors of MCS results are extremely small and are thus not showed. The impact of Doppler broadening of Compton scattering was also tested but showed to be negligible on both the photon flux and KERMA, and it is thus not presented.

As seen from Figs. 4–6, the photon spectrum retains about the same shape in the different material regions throughout the burnup steps. Turning off the simulation of atomic relaxation causes significant discrepancies in the photon flux at low energies below 116 keV (corresponding to the maximum energy of a fluorescence photon after the ejection of a K-shell electron in uranium through photoelectric effect [44]). Turning off the simulation of Bremsstrahlung decreases the number of photons overall at all energies with a bigger reduction at low energy (about 20%–40%) and a reduction of several percents in the range few hundred keV up to 1 or 2 MeV.

As seen in Table 2, the photon KERMA in the fuel is virtually unaffected by different photon physics. Without atomic relaxation, the difference for photon KERMA in the cladding reaches up to −5%. The lack of fluorescence photons emitted from the fuel is the main contributor for this difference. The photon KERMA in the water is less affected by fluorescence photons. Turning off Bremsstrahlung gives a 0.5% impact on the photon KERMA in the cladding and 1.5% impact on the photon KERMA in the water.

The multigroup photon heat production cross section generated by NJOY for STREAM are illustrated in Fig. 7 for the four relevant elements of the VER 1B pin: hydrogen, oxygen, zirconium and uranium. As seen in Fig. 7, zirconium and uranium have much lower heat production cross sections in the middle energy range (from 100 keV to several MeV) than at lower and higher energies. This middle energy range roughly matches the range of Bremsstrahlung photons in the VERA 1B pin cell and as a result, the impact of lack of Bremsstrahlung photons is lower in uranium and zirconium than the impact of a lack of fluorescence photons. In contrast, hydrogen possesses much lower heat production cross sections in the low-energy region of fluorescence photons and exhibits increasing heat production cross sections with increasing photon energies. Therefore, photons from Bremsstrahlung have more impact than the fluorescence photons in the heating of water.

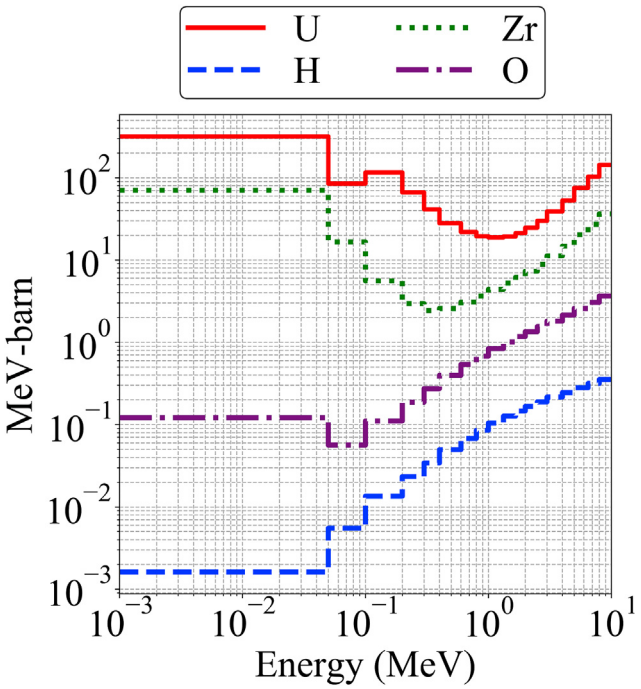

Fig. 7. Multigroup heat production cross section from NJOY.

The photon flux derived from STREAM fixed-source solver is compared to the MCS photon flux in "*All off*" case (to ensure consistent physics between the two codes) in Fig. 8 and a good agreement is observed between the two codes. The photon KERMA calculated by STREAM by means of the heat production cross section is then compared to the photon KERMA calculated by MCS in the "*All on*" case in Table 3. A 5% underestimation of the photon KERMA in the cladding and an agreement within 1.5% for the fuel and water are observed throughout depletion. This agreement is considered satisfying for TH feedback and depletion applications where the energies deposited in the fuel and in the water are more

Table 2
MCS photon KERMA for VERA 1B with different photon physics options.

Material	Photon physics options in MCS	BOC		MOC		EOC	
		MCS[a]	Rel. Diff.[b] (%)	MCS[a]	Rel. Diff.[b] (%)	MCS[a]	Rel. Diff.[b] (%)
Fuel	*All on*	4.998	–	4.953	–	4.914	–
	Atomic relaxation off	5.026	0.56	4.979	0.53	4.939	0.52
	Bremsstrahlung off	5.004	0.12	4.958	0.11	4.919	0.11
	All off	5.030	0.64	4.983	0.61	4.943	0.61
Cladding	*All on*	0.536	–	0.549	–	0.554	–
	Atomic relaxation off	0.508	−5.15	0.523	−4.68	0.529	−4.53
	Bremsstrahlung off	0.533	−0.52	0.546	−0.43	0.552	−0.38
	All off	0.508	−5.24	0.523	−4.68	0.528	−4.58
Water	*All on*	0.301	–	0.310	–	0.313	–
	Atomic relaxation off	0.301	−0.13	0.310	−0.13	0.313	−0.08
	Bremsstrahlung off	0.298	−0.99	0.307	−1.05	0.310	−1.08
	All off	0.298	−1.32	0.305	−1.46	0.309	−1.47
Total	*All on*	5.835	–	5.811	–	5.780	–
	Atomic relaxation off	″	–	″	–	″	–
	Bremsstrahlung off	″	–	″	–	″	–
	All off	″	–	″	–	″	–

[a] MeV per neutron source.
[b] *Rel. Diff.* takes MCS "*All on*" as reference.

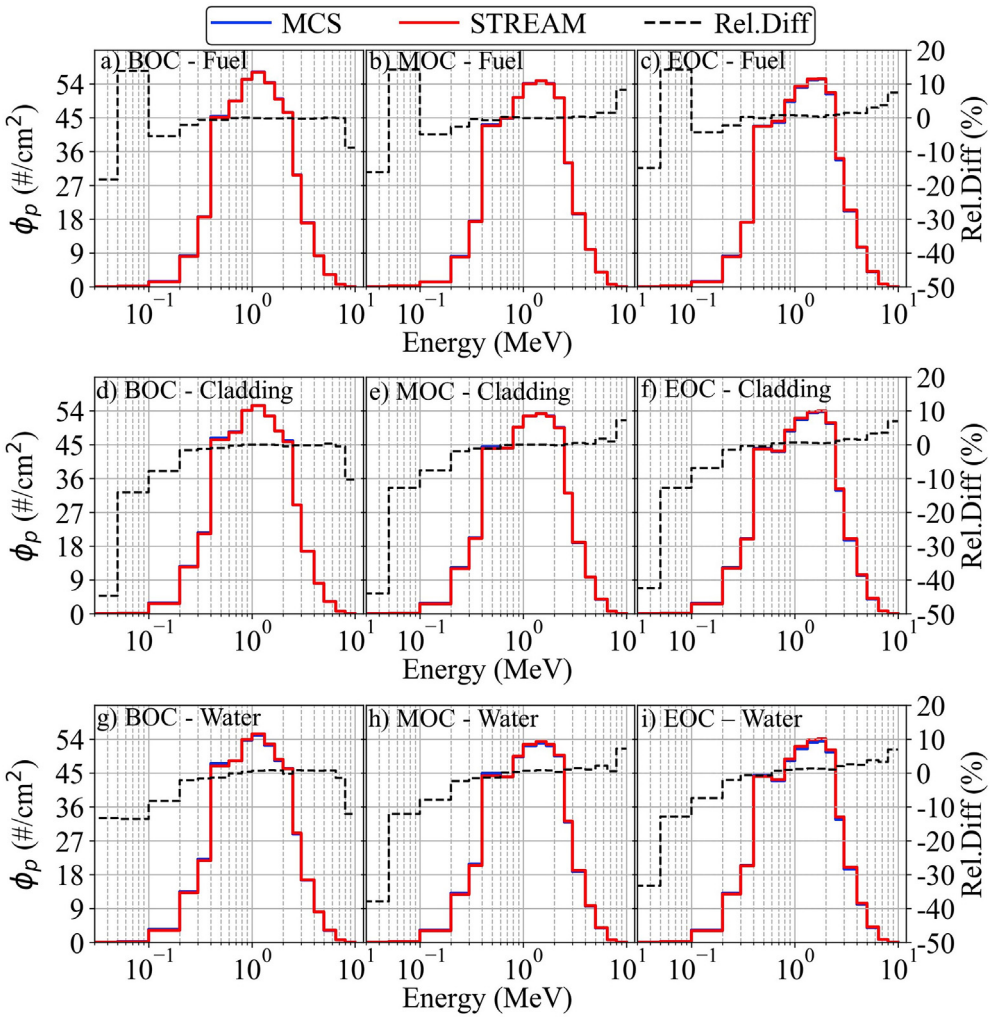

Fig. 8. Comparison of photon flux of VERA 1B between STREAM and MCS "*All off*" case (normalized by one neutron source).

Table 3
Comparison of photon KERMA between STREAM and MCS "*All on*".

Burnup	Material	STREAM[a]	Rel. Diff. to MCS "All on" (%)
BOC	Fuel	5.025	0.54
	Cladding	0.506	−5.56
	Water	0.299	−0.95
	Total	5.830	−0.09
MOC	Fuel	4.987	0.69
	Cladding	0.522	−4.82
	Water	0.308	−0.75
	Total	5.817	0.09
EOC	Fuel	4.977	1.29
	Cladding	0.531	−4.03
	Water	0.313	−0.20
	Total	5.821	0.69

[a] MeV per neutron source.

Table 4
k_{eff} of VERA 2B and VERA 2P at BOC, MOC and EOC.

Problem	Burnup	MCS	STREAM	Difference (pcm)
VERA 2B	BOC	1.18291 ± 0.00004	1.18204	−87 ± 4
	MOC	0.90010 ± 0.00003	0.90087	77 ± 3
	EOC	0.77322 ± 0.00003	0.77438	116 ± 3
VERA 2P	BOC	0.92677 ± 0.00003	0.92734	57 ± 3
	MOC	0.87890 ± 0.00003	0.87944	54 ± 3
	EOC	0.74304 ± 0.00003	0.74447	143 ± 3

important quantities than the energy deposited in the cladding.

3.2. VERA 2B & 2P: 2D lattice problem

The VERA 2B problem only contains standard fuel pins with 3.1% w/o enrichment whereas the VERA 2P includes several gadolinia pins, which are strong neutron absorbers and strong gamma emitters. Similar power density and burnup steps are used as in the VERA 1B case and the k_{eff} comparison throughout depletion between STREAM and MCS is shown in Table 4. The photon KERMA calculated by STREAM at BOC, MOC and EOC are shown in Fig. 9 for VERA 2B, respectively Fig. 11 for VERA 2P. The relative differences of STREAM's photon KERMA against MCS "*All on*" are displayed in Fig. 10 for VERA 2B, respectively Fig. 12 for VERA 2P (absolute statistical uncertainty of MCS photon KERMA are in the order of 10^{-2} keV per neutron source for fuel and of 10^{-3} keV per neutron source for cladding and water).

The agreement between STREAM and MCS for VERA 2B shows a similar trend during depletion as in the case of VERA 1B. In the absence of gadolinia pins, the photon KERMA has a relatively flat distribution in the lattice. Gadolinium (Gd) in VERA 2P is a strong neutron absorber capable of emitting 7.8 MeV gamma after a radiative neutron capture [43]. Such high energy photon can create a series of secondary photons by means of Bremsstrahlung and atomic relaxation which are assumed to be locally deposited in

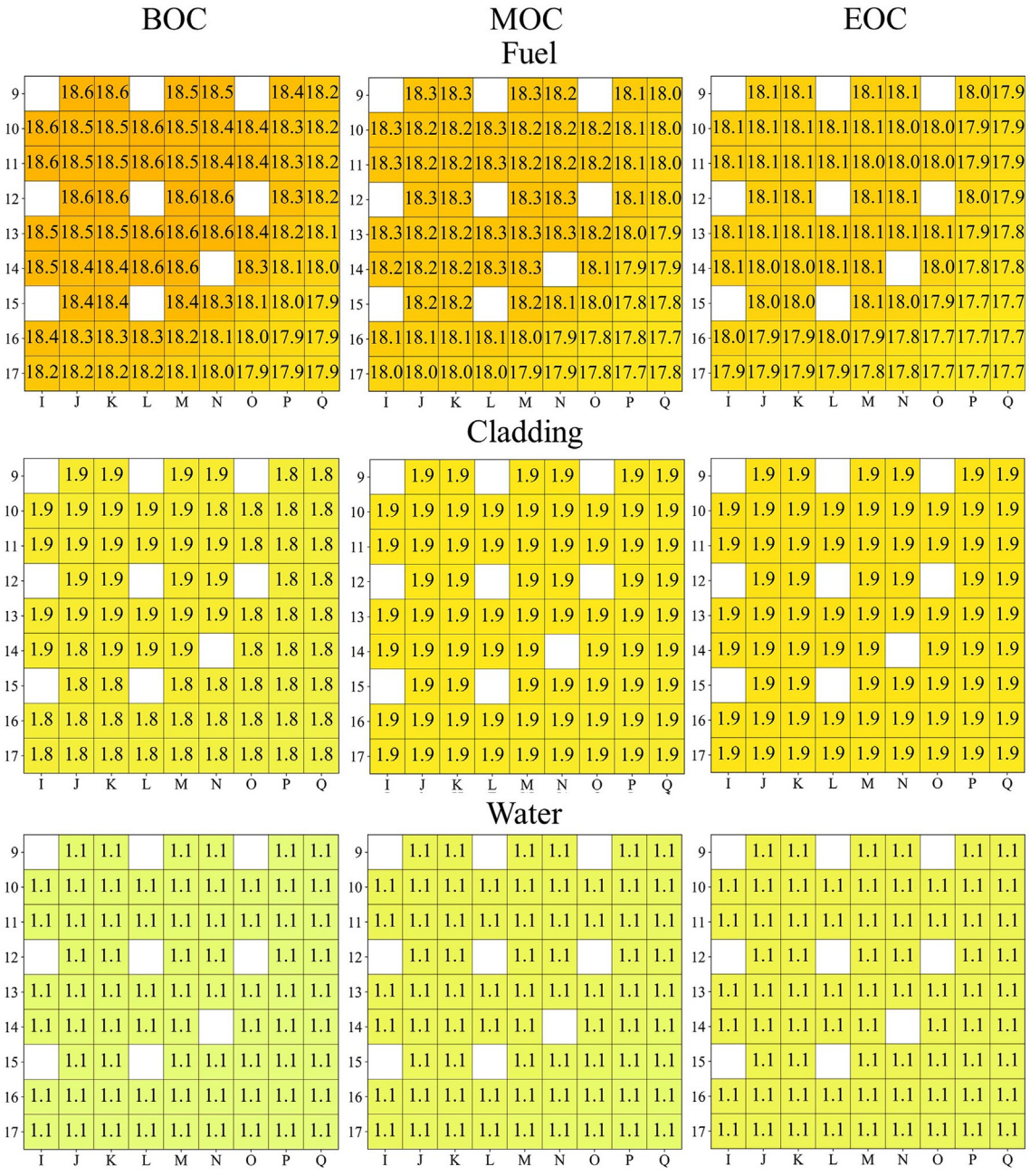

Fig. 9. Photon KERMA from STREAM for VERA 2B (unit: keV per neutron source).

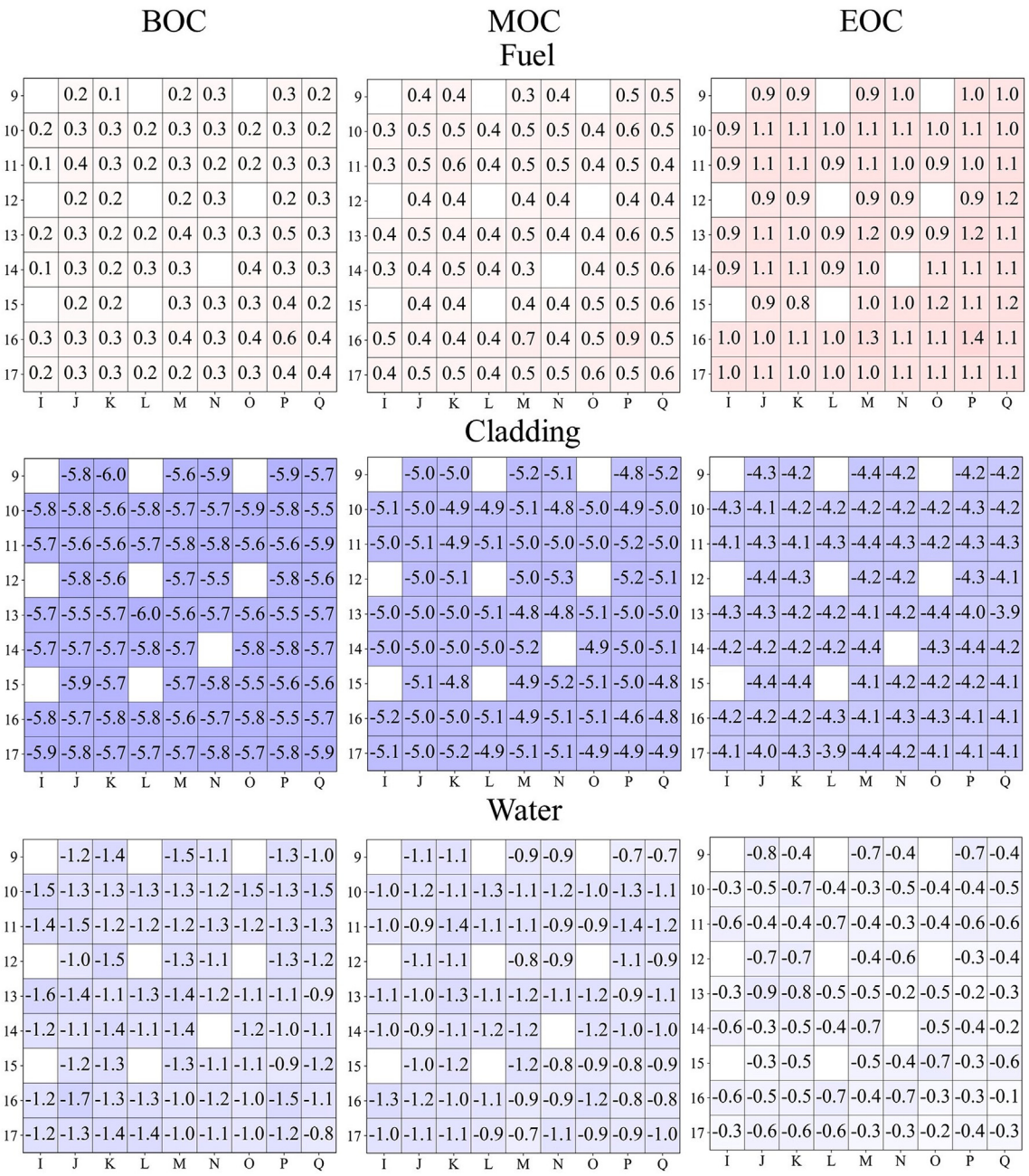

Fig. 10. Relative difference of photon KERMA from STREAM compared to MCS for VERA 2B (unit: %).

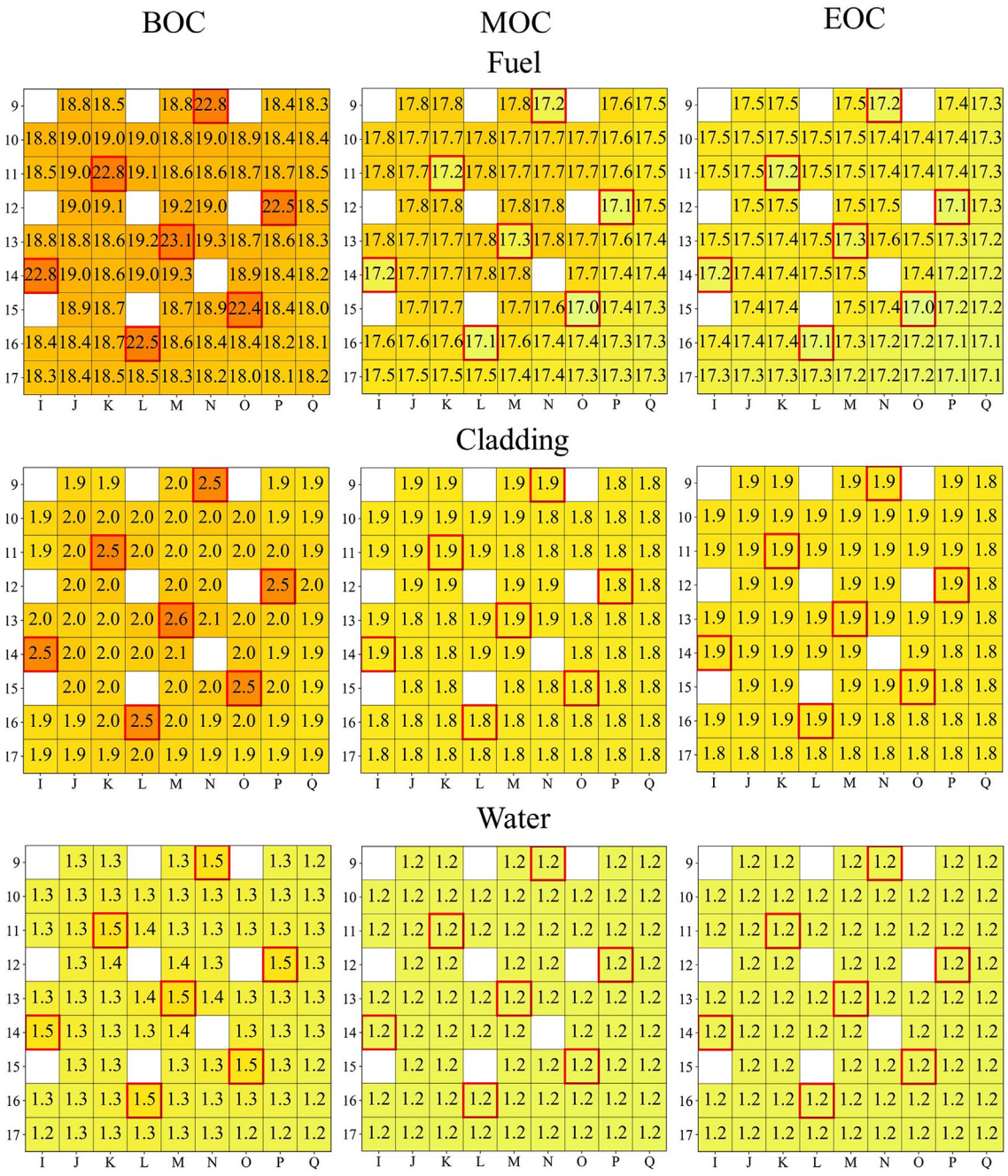

Fig. 11. Photon KERMA from STREAM for VERA 2P (unit: keV per neutron source, the gadolinia pins are marked by red squares). (For interpretation of the references to color in this figure legend, the reader is referred to the Web version of this article.)

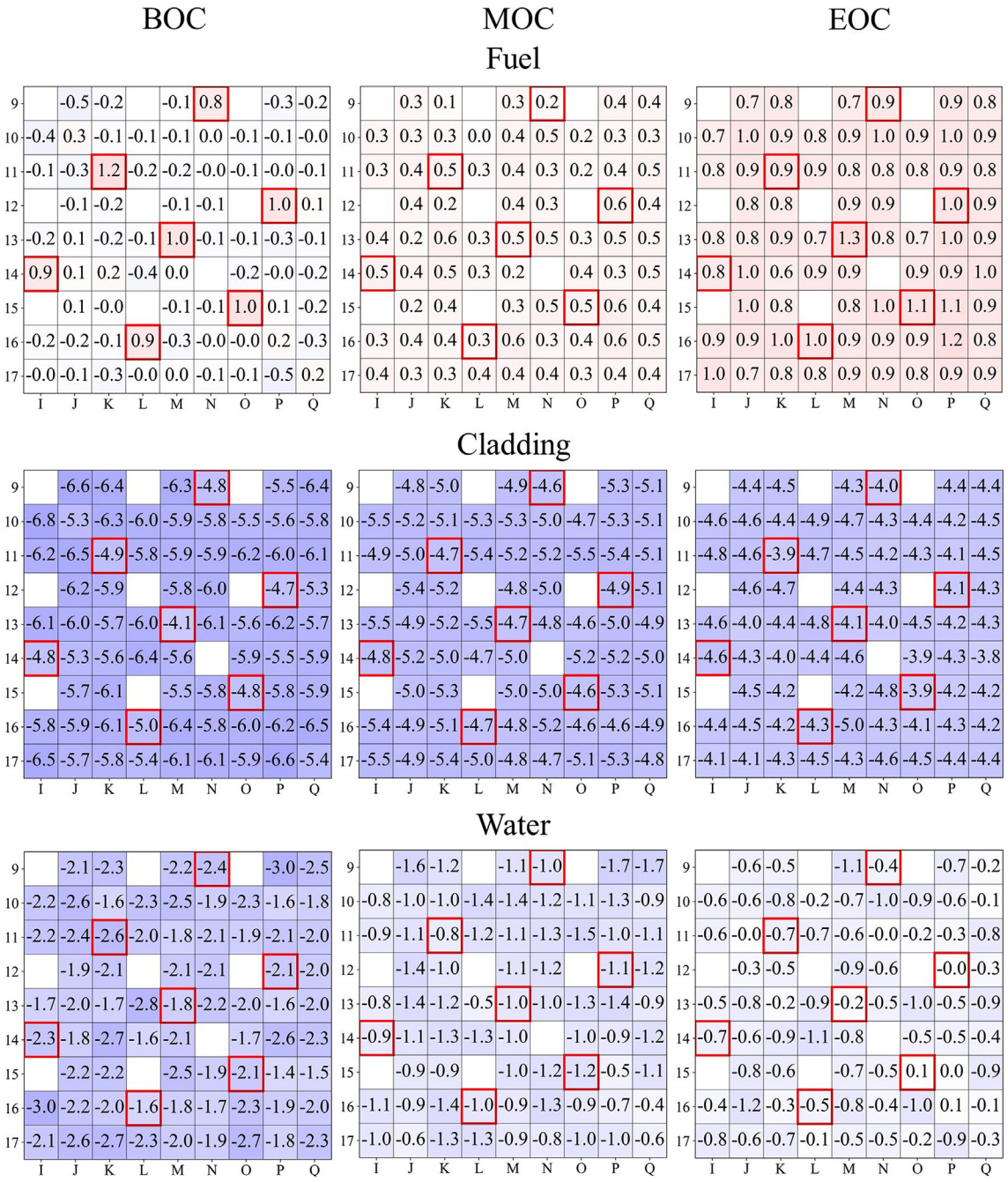

Fig. 12. Relative difference of photon KERMA from STREAM compared to MCS for VERA 2P (unit: %, the gadolinia pins are marked by red squares). (For interpretation of the references to color in this figure legend, the reader is referred to the Web version of this article.)

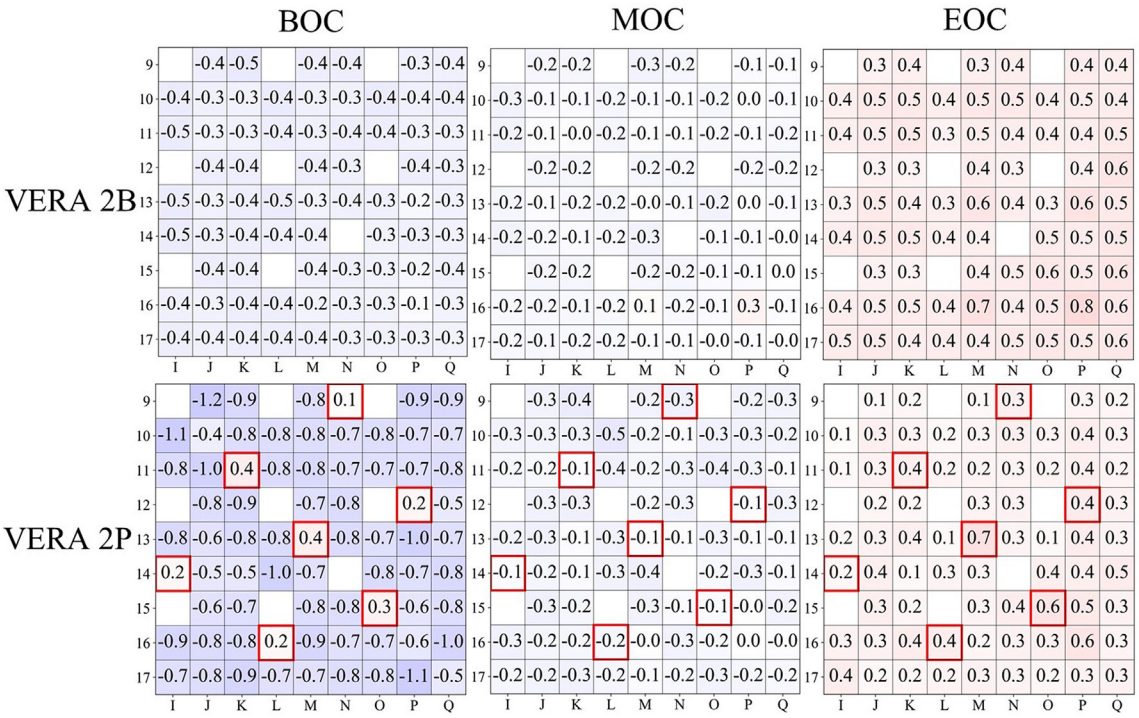

Fig. 13. Relative difference for pin-wise photon KERMA between STREAM and MCS (unit: %, the gadolinia pins are marked by red squares). (For interpretation of the references to color in this figure legend, the reader is referred to the Web version of this article.)

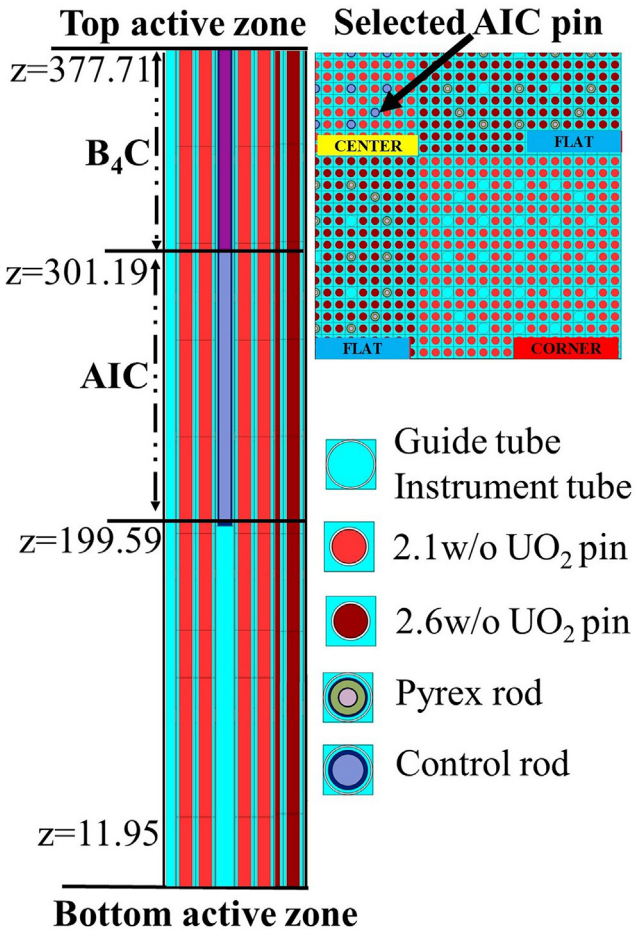

Fig. 14. Layout of VERA 4 problem in a quarter symmetry (dimension is not-to-scale).

STREAM, hence an overestimation of 1% observed in the gadolinia pins at BOC in Fig. 12 whereas an underestimation of −6% and −2% are observed at the same burnup for cladding and water, respectively. After the gadolinia burnout, the relative differences to MCS of the VERA 2P problem become similar to that of VERA 2B as seen at MOC and EOC. The comparison of pin-wise total photon KERMA for VERA 2B and VERA 2P between STREAM and MCS is presented in Fig. 13 and shows a good agreement between the two codes within 1.5%.

3.3. *VERA 4: 3D 3-by-3-assembly problem with half-inserted control rods*

The VERA 4 benchmark is a 3D problem consisting of nine 17 × 17 fuel assemblies arranged in a 3 × 3 square with a control rod (AIC/B_4C) inserted in the center fuel assembly and Pyrex rods placed in the water holes of the flat assemblies. The fuel has two different enrichment levels of 2.1 and 2.6 w/o. The configuration of the selected VERA 4 problem is shown in Fig. 14 with control rods inserted half-way. Depletion is not considered for the 3D verification. Atomic relaxation and Bremsstrahlung physics are turned on in MCS for the comparison with STREAM.

For this problem, the k_{eff} for STREAM and MCS is 0.99496 and 0.99546 ± 0.00002, respectively, resulting in a difference of −51 pcm. The photon KERMA of all materials at a given axial height are summed together and this axial distribution for STREAM and MCS along the active zone is shown in Fig. 15. Rather large discrepancies are observed for the center assembly in the zone corresponding to the half-inserted AIC/B4C control rod as shown in Fig. 15a, whereas the flat assembly shows a difference of 3% in the same z range of AIC as shown in Fig. 15b. Apart from those discrepancies, the calculated photon KERMA is in agreement between MCS and STREAM. To emphasize the comparison, the pin-by-pin distribution of photon KERMA at the axial positions of $z = 251$ (AIC rod is present) and $z = 60$ (AIC rod is absent) is plotted

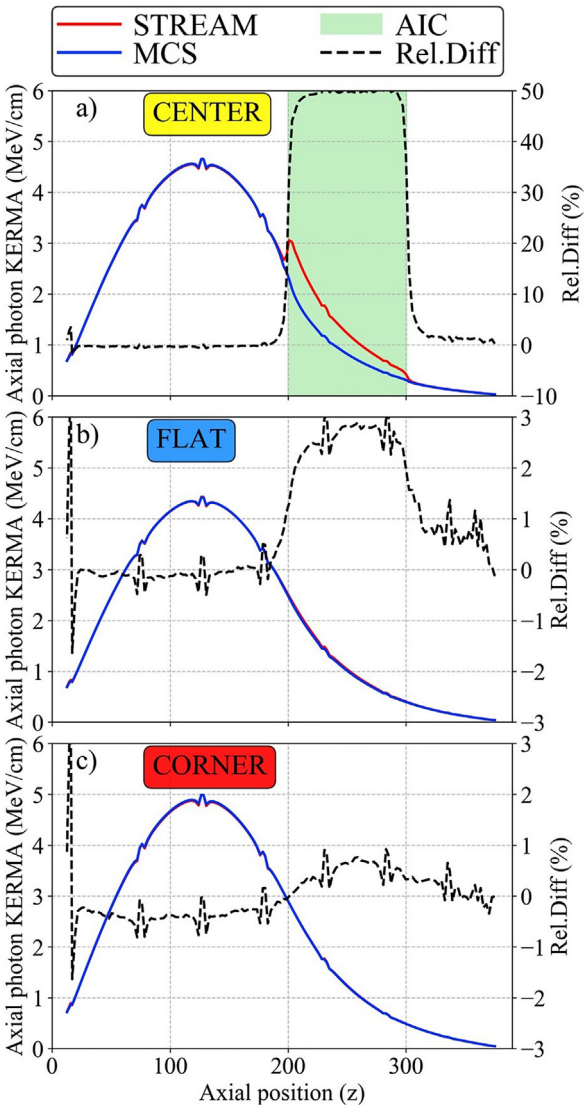

Fig. 15. Axial photon KERMA calculated by STREAM and MCS for the VERA 4 benchmark (normalized by one neutron source).

in Fig. 16a and b, respectively.

The AIC material of the control rod introduces much higher photon KERMA in STREAM in the center assembly and the pins neighboring the center assembly as seen in Fig. 16a whereas a good agreement between MCS and STREAM is observed in the absence of the AIC control rod in Fig. 16b. The AIC pin marked in Fig. 14 is selected for further studies to determine the reason for the differences observed in Figs. 15a and 16a. As shown in Fig. 17a, the gamma source in the AIC material is significantly higher in STREAM compared to MCS and this difference in the gamma source eventually led to the observed differences in the photon KERMA. The difference in the gamma source can be explained by the fact that the equivalence theory is applied for resonance treatment of neutron multi-group cross-sections for non-fuel pins instead of the pin-based point wise energy slowing down in STREAM [17]. The range highlighted by the green color in the neutron spectrum of Fig. 17b is the main contributor to the differences in the gamma source as this range coincides with the resonance peak of the gamma production cross section for Ag^{109} indicated in Fig. 17c (Ag^{109} is one of the major components of the AIC material with a thermal capture cross section of about thousand barns). It is worth noting that unlike the silver and cadmium elements in AIC, the boron in B_4C, Pyrex and coolant are free from resonance in the intermediate energy range and therefore they do not suffer from the same problem as silver and cadmium do. Future improvements on the resonance treatment for neutron multigroup cross section would alleviate some of the current issues observed in STREAM for non-fuel pins when absorbing material such as AIC is inserted.

4. Short analysis of photon transport impact on depletion calculations with TH feedback

The impact of explicit photon transport on depletion calculations with TH feedback is studied on the VERA 5 benchmark shown in Fig. 18 (2D quarter core with Pyrex rods, core baffle and barrel). The STREAM calculations with explicit photon transport are compared against STREAM calculations using the on-the-fly Kappa (OTFK). The OTFK method is described in references [45,46] and does not transport photons, but instead relies on three assumptions to calculate the pin power needed in depletion and feedback calculations. First, the energies of prompt and delayed gamma from fission events are assumed to be deposited locally and are thus included in Kappa values. Second, the gamma energies from neutron capture reactions in fission products, cladding, moderator are computed and summed together, then averaged by the total fission rate and incorporated into the Kappa values for power calculation. This approach comes down to dividing into each fuel pin, proportionally to the fission rate in that pin, the total gamma energy emitted by the neutron captures in the system. The total amount of gamma energy in a system is thus preserved with the OTFK method. Third and finally, the fraction of photon energy deposited in the coolant is provided by use preference (a fraction of 2.6% from Refs. [47,48] is used in STREAM).

A depletion calculation with Critical Boron Concentration (CBC) search, Equilibrium Xenon calculation (EQXE) and TH feedback using simple TH1D model is conducted with photon transport (including delayed fission gammas) and with the OTFK method (i.e., without photon transport) for the VERA 5 2D problem. Thermal expansion feedback is not applied. The energy deposition from neutron slowing down is explicitly calculated in STREAM by a simple approach described in Ref. [47] in photon transport calculation mode. In photon transport mode, the heat source in the cladding due to the photon energy deposition there is considered in the TH1D solver. The problem was depleted to 16.939 MWd/kg, corresponding to the expected cycle length of 441 Effective Full Power Days (EFPDs) for the cycle one of the VERA core [22]. Calculations are performed on the same machine using Intel Xeon 3.4 GHz (8 processors) with OpenMP parallelization and the computing time with memory consumption between OTFK method and photon transport is compared in Table 5. Calculation with photon transport is indicated as WP (with photons) for the rest of the paper.

Pin-wise power distribution calculated with photon transport and the relative differences defined as $\left(\frac{WP}{OTFK}-1\right)\times 100\%$ at 0 MWd/kg (BOC) and 16.939 MWd/kg (EOC) are presented in Fig. 19. When photons are transported, slightly higher pin power (about +0.8% to +1.3%) is observed in the pins surrounding the Pyrex rods compared to OTFK at BOC. This is expected as Pyrex contains ^{10}B, a strong neutron absorber that emits capture gammas of energy ~0.45 MeV [43]. With the assumptions in the OTFK method, these gamma energies have been spread out in the entire problem whereas in explicit photon transport, these gamma rays are transported out of Pyrex and get absorbed in the neighboring

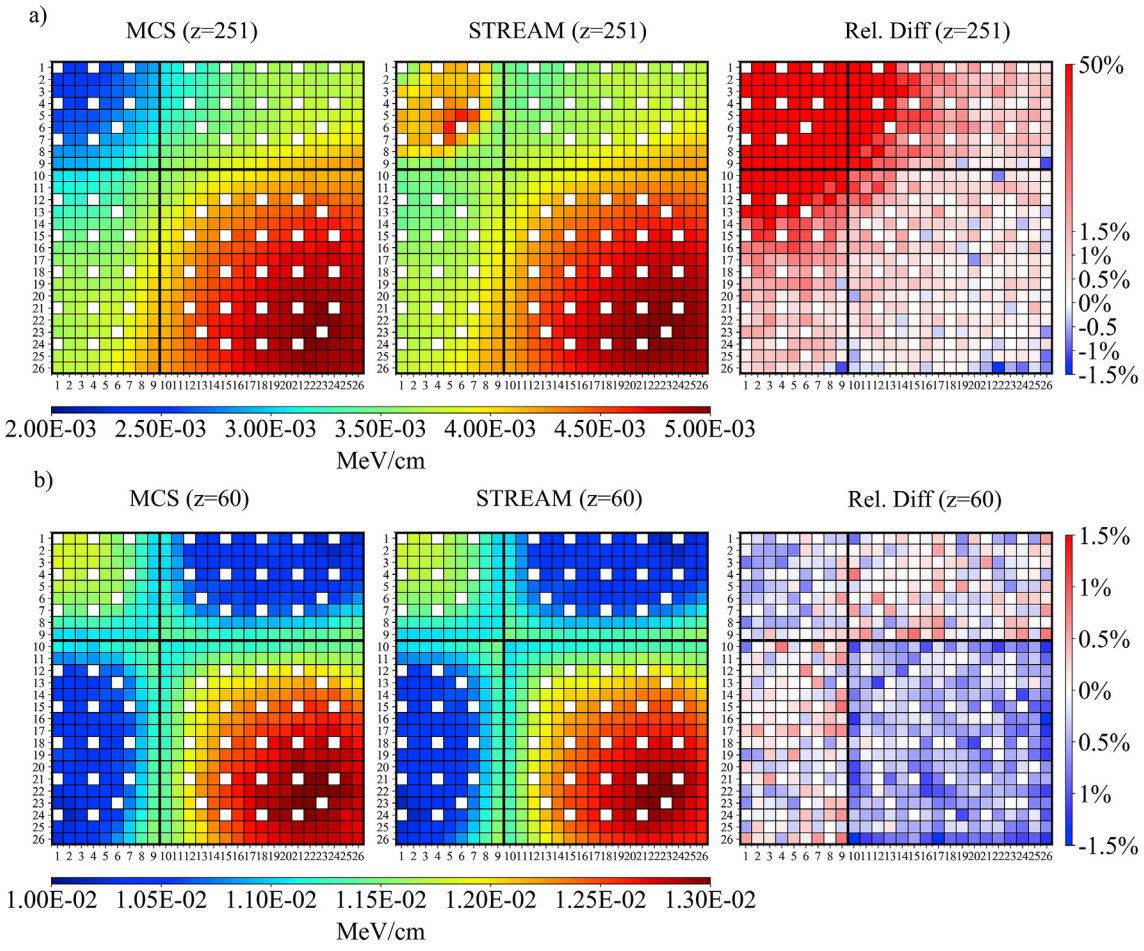

Fig. 16. Photon KERMA of VERA 4 benchmark at z = 251(a) and z = 60(b).

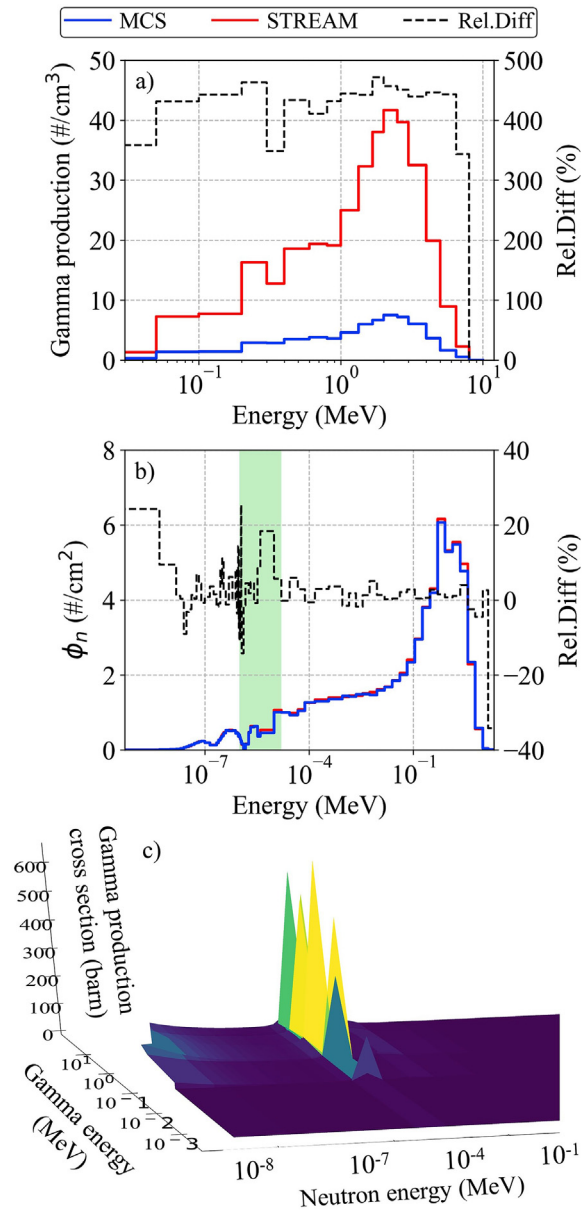

Fig. 17. Neutron flux and gamma source in the selected AIC pin of VERA 4 and the gamma production matrix of ^{109}Ag.

pins. Slightly higher pin power (+0.2% to +1.3% at BOC and +0.4% to +0.7% at EOC) is also observed at the periphery of non-Pyrex assemblies located at core center when photons are transported compared to OTFK. This increase can be explained by the fact that peripheral pins of non-Pyrex assembly have lower power compared to internal pins of the same assembly or compared to peripheral pins of adjacent Pyrex assemblies. More neutron/gammas are therefore generated in internal pins of non-Pyrex assemblies or peripheral pins of Pyrex assemblies than in peripheral pins of non-Pyrex assemblies, but those neutron/gammas are locally deposited in OTFK mode whereas they are transported to neighboring pins in photon transport mode, thus inducing higher power in peripheral pins of non-Pyrex assemblies. In contrast, slightly lower pin power (about −0.1% to −1.8% at BOC and −0.7% to −2.6% at EOC) are observed for the assemblies located at the edge of the core in photon transport mode compared to OTFK, due to the neutron/photon leakage calculated precisely in photon transport mode

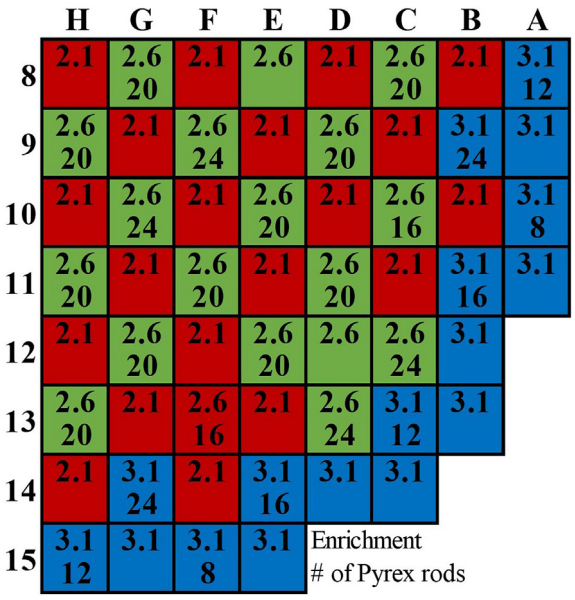

Fig. 18. Layout of VERA 5 2D case.

Table 5
Time and memory consumption of OTFK and photon transport (WP) for VERA 5 2D problem.

Mode	Computing time (minutes)	Memory (GB)
WP	196	11.2
OTFK	144	9.4

whereas fission gammas and fission neutrons deposit their energies locally in OTFK mode.

Closer analysis of the energy deposition in each material of selected pins indicated in Fig. 20 is presented in Table 6. The pin ID, for example H10-Q09 in Table 6, represents the pin Q09 of assembly H10. For comparison purposes, the energy deposited in the coolant with OTFK is calculated by multiplying the total pin power by 2.6% and the energy deposited in the fuel is obtained by multiplying the total pin power by 97.4%. It is shown that for most fuel pins, less energy is deposited in the fuel and coolant regions in WP mode compared to OTFK. This better prediction of the energy repartition between the materials explains why the fuel temperature decreases in general in photon transport mode. The pin-by-pin average fuel temperature are mostly lower in photon transport mode with a maximum decrease of 9° for one pin. The Maximum Fuel Centerline Temperature is reduced by ~12° compared to OTFK at BOC (photon transport 1272.1 K vs OTFK 1284.5 K) and 13° at EOC (1278.8 K vs OTFK 1291.5 K). The coolant temperature does not show any noticeable difference when photon transport is turned on compared to OTFK. The changes in fuel temperatures for this VERA 2D core are small with photon transport, and therefore, the changes in cross sections by Doppler broadening are trivial. The maximum relative difference in the total energy released between WP and OTFK mode is about ~0.4% during depletion. The total energy released is preserved in both modes and thus, the number densities of nuclides in fuel regions do not show any noticeable differences during depletion with photon transport compared to OTFK. The Critical Boron Concentration is also similar in both calculation modes. The relative difference in Power Peaking Factor between WP and OTFK mode is highest at BOC, approximately −0.5%.

The fraction of energy deposited in each material for each VERA problem is summarized in Table 7. The fraction of gamma energy is

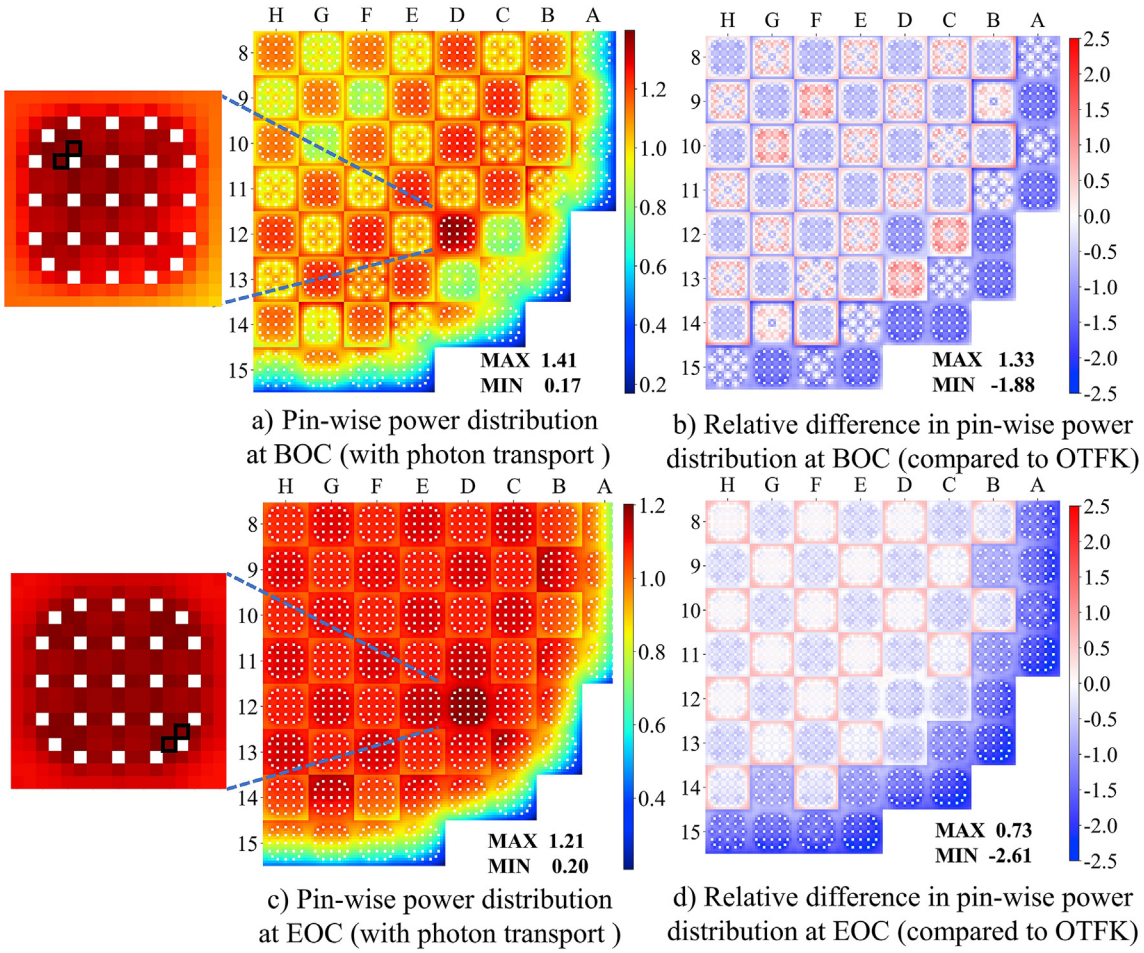

Fig. 19. Normalized pin-wise power distribution with photon transport (a, c) and relative difference (unit: %) compared to OTFK method (b, d) for VERA 5 2D problem (hot spots marked by black squares).

obtained by dividing the gamma energy deposited in each material by the total energy released in the problem and the fraction of energy deposited in each material is computed by dividing the total energy deposited in each material by the total energy released in the problem. Depletion is not considered for VERA 4. The fractions of energy deposition for VERA 2B problem are in good agreement with values calculated by OpenMC and reported in Ref. [49]. It is observed from the results of the VERA 2D problems calculated with photon transport that gamma energy accounts for around 10% of the released energy and that ~2.6% of the total energy released is deposited in the coolant, which agrees with the values reported in Refs. [47,48].

5. Conclusions and perspectives

A photon transport module has been implemented in the deterministic transport code STREAM for 2D and 3D calculations with a photon library based on ENDF/B-VII.1. The sources of prompt gammas from fission, radiative capture, inelastic scattering, and of delayed gammas from fission are calculated first as a result of solving the neutron transport equation, and then the photon flux is determined by solving the transport equation with fixed gamma sources. STREAM simulates coherent and incoherent photon scattering isotropically. The photoelectric effect and pair production are also included in which the positron annihilation is treated as $(\gamma, 2\gamma')$ scattering.

STREAM does not transport secondary photons from atomic relaxation and Bremsstrahlung and the energies of these photons are locally deposited through a standard NJOY assumption in the heat production cross section. In the absence of strong resonant neutron absorbers, a comparison between STREAM and MCS gives an agreement within 1.5% for photon KERMA in fuel and water and an underestimation of about 5% for photon KERMA in cladding, for a total pin-wise KERMA value agreement within 1.5%. The differences observed in the photon KERMA between STREAM and MCS are rooted in the nature of the computational methodologies of the two codes.

The impact of photon transport on depletion calculations with TH feedback of the VERA 2D core benchmarks was analyzed. The photon transport module in STREAM provides a better estimation of the fraction of energy deposited in coolant in TH feedback calculations. The pin-wise power calculated with explicit photon transport is reduced up to 2.6% for the pins adjacent to the baffle compared to On-The-Fly Kappa method, whereas pins at the periphery of inner assemblies and pins close to poison rods have slightly higher power level. The Maximum Fuel Centerline Temperature is reduced by ~13° and the average fuel temperature decreases at the maximum by ~9°. Slight change in Fq value occurs at BOC while other core parameters such as CBC, and coolant temperature do not show noticeable differences when photon transport is simulated explicitly. Calculation of VERA problems in STREAM indicates a ~10% of the total energy released as gammas

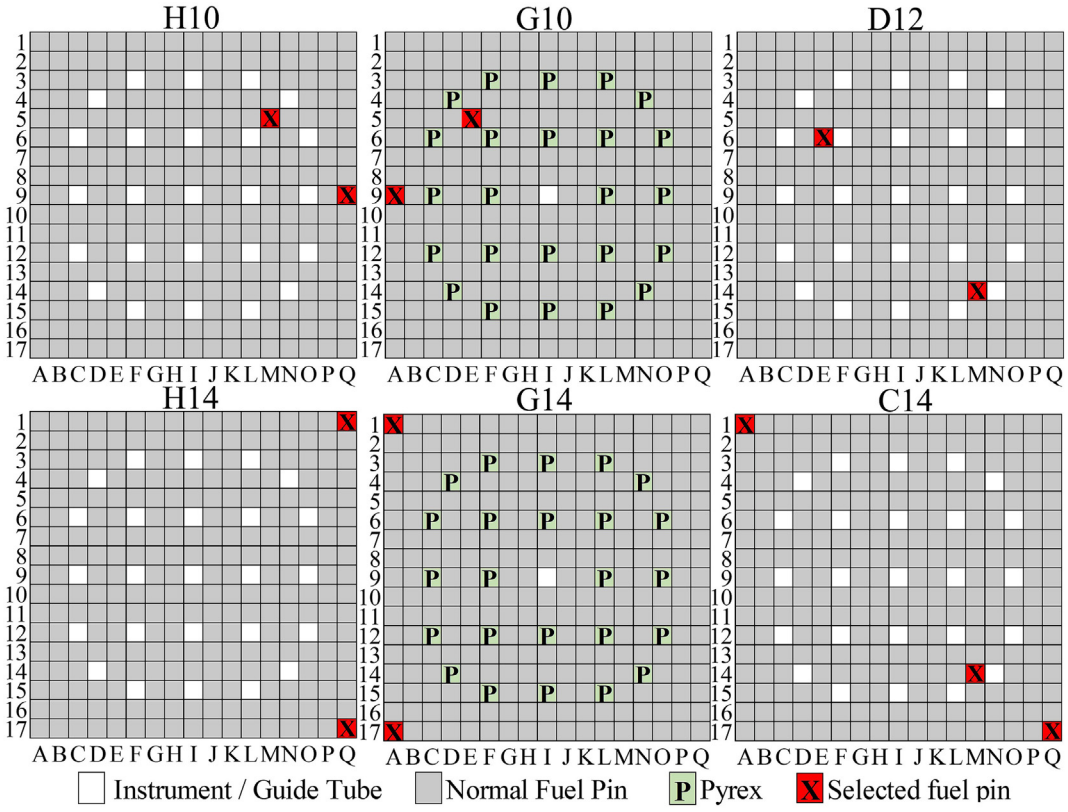

Fig. 20. Layout of selected assemblies and positions of selected pins for VERA 5 2D.

Table 6
Deposited power (in watts) in each material of selected pins from WP mode in comparison with those from OTFK.

Burnup	Pin ID	Fuel[a]	Coolant[a]	Clad[b]	Rel.Diff.[c] (%)	ΔT_f[d] (K)
BOC	H10-Q09	171.7 (−0.5)	4.1 (−10.1)	1.7	0.2	−1.3
	H10-M05	196.9 (−1.1)	4.3 (−19.1)	1.8	−0.7	−3.9
	G10-A09	185.4 (−1.2)	4.1 (−18.9)	1.6	−0.8	−3.9
	G10-E05	146.8 (+0.0)	3.7 (−5.3)	1.5	0.9	+0.2
	H14-Q01	178.0 (−0.1)	4.5 (−6.0)	1.8	0.7	−0.1
	H14-Q17	154.0 (+0.3)	4.0 (−1.7)	1.6	1.3	+1.0
	G14-A01	233.1 (−2.0)	4.5 (−28.7)	1.9	−1.9	−8.8
	G14-A17	198.5 (−1.6)	4.1 (−24.3)	1.7	−1.4	−5.5
	D12-E06	247.1 (−1.4)	5.1 (−24.4)	2.1	−1.2	−6.8
	D12-M14	229.1 (−1.5)	4.6 (−25.4)	1.9	−1.3	−6.6
	C14-A01	171.1 (−1.3)	3.6 (−21.9)	1.5	−1.0	−3.8
	C14-M14	72.4 (−1.8)	1.4 (−31.4)	0.6	−1.8	−0.3
	C14-Q17	30.2 (−0.8)	0.6 (−24.9)	0.3	−0.5	−1.9
EOC	H10-Q09	181.2 (−0.4)	4.4 (−9.6)	2.0	0.5	−1.7
	H10-M05	190.6 (−0.8)	4.3 (−15.6)	2.0	−0.1	−3.9
	G10-A09	192.9 (−0.9)	4.4 (−14.9)	2.0	−0.3	−4.8
	G10-E05	195.0 (−1.0)	4.4 (−16.0)	2.0	−0.4	−4.8
	H14-Q01	177.3 (−0.3)	4.4 (−7.5)	2.0	0.6	−1.2
	H14-Q17	156.9 (−0.2)	3.9 (−6.8)	1.8	0.7	−0.7
	G14-A01	203.5 (−1.4)	4.4 (−19.7)	2.0	−1.0	−7.9
	G14-A17	181.5 (−1.4)	4.0 (−19.4)	1.8	−0.9	−6.5
	D12-E06	211.5 (−1.1)	4.6 (−19.0)	2.2	−0.6	−6.4
	D12-M14	212.3 (−1.3)	4.5 (−20.7)	2.1	−0.8	−7.3
	C14-A01	172.6 (−1.4)	3.8 (−19.0)	1.7	−0.9	−5.8
	C14-M14	79.8 (−2.6)	1.4 (−35.8)	0.7	−2.6	−1.1
	C14-Q17	36.5 (−1.8)	0.7 (−33.6)	0.4	−1.7	−3.8

Bold font Hotspot.
[a] Rel. Diff. (WP/OTFK-1) × 100% is in brackets after the power value.
[b] Only available in WP.
[c] For total energy deposited in a selected pin (WP/OTFK-1) × 100%.
[d] Change in fuel temperature (WP-OTFK).

Table 7
Fraction of energy deposited in VERA problems obtained by WP.

Burnup	Problem	Fraction of deposited energy in each material compared to the total energy released (%)					
		Fuel		Cladding		Coolant	
		Gamma	All[a]	Gamma	All[a]	Gamma	All[a]
BOC	VERA 2B	8.06	96.51	0.86	1.00	0.81	2.49
	VERA 2P	8.90	96.23	0.99	1.12	0.94	2.65
	VERA 4	7.87	96.32	0.88	1.02	0.96	2.66
	VERA 5	7.86	96.45	0.89	1.05	0.79	2.50
MOC	VERA 2B	8.83	96.22	0.98	1.13	0.83	2.65
	VERA 2P	8.69	96.07	0.97	1.11	0.94	2.82
	VERA 5	8.31	96.32	0.96	1.13	0.75	2.55
EOC	VERA 2B	9.18	96.08	1.04	1.19	0.86	2.73
	VERA 2P	9.04	95.92	1.02	1.17	0.99	2.91
	VERA 5	8.61	96.32	1.01	1.18	0.66	2.49

[a] Neutron, gamma, fission fragments, etc.

and ~2.6% of the total energy deposited in the coolant.

Future STREAM studies will focus on the analysis of several Korean-designed reactors containing gadolinia poison to provide validation elements of the new photon transport mode against measured data. At this occasion, the necessity of developing methodologies to simulate the transport of fluorescence and Bremsstrahlung photons in the presence of strong neutron absorbers will be assessed. Code optimization is also required to reduce the calculation time of TH feedback runs involving explicit photon transport.

Declaration of competing interest

The authors declare that they have no known competing financial interests or personal relationships that could have appeared to influence the work reported in this paper.

Acknowledgements

This work was supported by Korea Institute of Energy Technology Evaluation and Planning (KETEP) grant funded by the Korea government (MOTIE) (20206510100040).

Appendix A. Supplementary data

Supplementary data to this article can be found online at https://doi.org/10.1016/j.net.2022.02.004.

References

[1] J.R. Lamarsh, A.J. Baratta, Introduction to Nuclear Engineering, Prentice Hall, Upper Saddle River, NJ, 2001.
[2] J. Sterbentz, Q-value (MeV/fission) Determination for the Advanced Test Reactor, Idaho National Laboratory (INL), 2013. No. INL/EXT-13-29256.
[3] L. Ghasabyan, K. Mikityuk, J. Krepel, S. Pelloni, Use of Serpent Monte-Carlo code for development of 3D full-core models of Gen-IV fast spectrum reactors and preparation of safety parameters/cross-section data for transient analysis with FAST code system, in: Proceedings of International Conference on Fast Reactors and Related Fuel Cycles: Safe Technologies and Sustainable Scenarios (FR13), Paris, 2013. March.
[4] J.L. Peterson-Droogh, R.H. Howard, Current neutronic calculation techniques for modeling the production of Ir-192 in HFIR, in: Proceedings of the PHYSOR, Cancun, Mexico, 2018. April 22-26.
[5] K.S. Kim, K.T. Clarno, Y. Liu, X. Wang, W.R. Martin, B.S. Collins, Neutron Capture Energies for Flux Normalization and Approximate Model for Gamma-Smeared Power, Oak Ridge National Lab (ORNL), 2018. No. ORNL/SPR-2017/471.
[6] C. Liegeard, A. Calloo, G. Marleau, Impact of photon transport on power distribution, in: Proceedings of the International Conference on Mathematics and Computational Methods Applied to Nuclear Science and Engineering - M&C 2017, Jeju, Korea, 2017. April 16-20.
[7] AREVA NP INC, The ARCADIA® Reactor Analysis System for PWRs Methodology Description and Benchmarking Results, Tech. rep., Areva NP Inc, 2010. March.
[8] J.T. David, ICRU report 85: Fundamental quantities and units for ionizing radiation, Radiat. Protect. Dosim. 150 (4) (2012) 550–552.
[9] R. Sanchez, I. Zmijarevic, M. Coste-Delclaux, E. Masiello, S. Santandrea, E. Martinolli, L. Villate, N. Schwartz, N. Guler, APOLLO2 year 2010, Nucl. Eng. Technol. 42 (5) (2010) 474–499.
[10] R.J.J. Stamml'er, et al., HELIOS Methods, Studsvik Scandpower, 2003.
[11] H.N. M Gheorghiu, J. Rhodes, CASMO-5 gamma library, in: Proceedings of Advances in Nuclear Fuel Management IV, South Carolina, USA, 2009. April 12-15.
[12] B.A. Lindley, J.G. Hosking, P.J. Smith, D.J. Powney, B.S. Tollit, T.D. Newton, R. Perry, T.C. Ware, P.N. Smith, Current status of the reactor physics code WIMS and recent developments, Ann. Nucl. Energy 102 (2017) 148–157.
[13] S. Jae, N. Choi, H.G. Joo, Implementation and verification of explicit treatment of neutron/photon heating in nTRACER, in: Proceedings of ICAPP 2020, Abu Dhabi, UAE, 2020. March 15-19.
[14] X. Wang, Y. Liu, W. Martin, S. Stimpson, Implementation of 2D/1D gamma transport and gamma heating capability in MPACT, in: Proceedings of PHYSOR2020, Cambridge, UK, 2020. March 29 - April 02.
[15] G. Rimpault, D. Bernard, D. Blanchet, G.C. Vaglio, S. Ravaux, A. Santamarina, Needs of accurate prompt and delayed γ-spectrum and multiplicity for Nuclear Reactor Designs, Phys. Procedia 31 (2012) 3–12.
[16] S. Choi, W. Kim, J. Choe, W. Lee, H. Kim, B. Ebiwonjumi, E. Jeong, K. Kim, D. Yun, H. Lee, D. Lee, Development of high-fidelity neutron transport code STREAM, Comput. Phys. Commun. 264 (2021), 107915.
[17] S. Choi, C. Lee, D. Lee, Resonance treatment using pin-based pointwise energy slowing-down method, J. Comput. Phys. 330 (2017) 134–155.
[18] J. Choe, S. Choi, P. Zhang, J. Park, W. Kim, H.C. Shin, H.S. Lee, J.E. Jung, D. Lee, Verification and validation of STREAM/RAST-K for PWR analysis, Nucl. Eng. Technol. 51 (2) (2019) 356–368.
[19] B. Ebiwonjumi, S. Choi, M. Lemaire, D. Lee, H.C. Shin, H.S. Lee, Verification and validation of radiation source term capabilities in STREAM, Ann. Nucl. Energy 124 (2019) 80–87.
[20] M.B. Chadwick, M. Herman, P. Obložinský, M.E. Dunn, Y. Danon, A.C. Kahler, D.L. Smith, B. Pritychenko, G. Arbanas, R. Arcilla, R. Brewer, ENDF/B-VII. 1 nuclear data for science and technology: cross sections, covariances, fission product yields and decay data, Nucl. Data Sheets 112 (12) (2011), 2887-2996.
[21] A.C. Kahler III, R. Macfarlane, NJOY2016, Los Alamos National Lab (LANL), NJOY, NJOY16; 005075MLTPL00, Los Alamos, NM (United States), 2016.
[22] B.A. Godfrey, VERA Core Physics Benchmark Progression Problem Specifications, Revision 4, CASL Technical Report, 2014. CASL-U-2012-0131-004.
[23] H. Lee, W. Kim, P. Zhang, M. Lemaire, A. Khassenov, J. Yu, Y. Jo, J. Park, D. Lee, MCS–A Monte Carlo particle transport code for large-scale power reactor analysis, Ann. Nucl. Energy 139 (2020), 107276.
[24] K. Kim, M. Lemaire, N.N.T. Mai, W. Kim, D. Lee, Generation of a multigroup gamma production and photon transport library for STREAM, in: Transactions of the Korean Nuclear Society Virtual Spring Meeting, 2020. July 09-10.
[25] R.E. Macfarlane, D.W. Muir, D. C George, NJOY99.0 Code System for Producing Pointwise and Multigroup Neutron and Photon Cross Sections from ENDF/B Data, Los Alamos National Laboratory, 2000. PSR-480.
[26] J. Leppänen, M. Pusa, T. Viitanen, V. Valtavirta, T. Kaltiaisenaho, The Serpent Monte Carlo code: status, development and applications in 2013, Ann. Nucl. Energy 82 (2015) 142–150.
[27] P.K. Romano, N.E. Horelik, B.R. Herman, A.G. Nelson, B. Forget, K. Smith, OpenMC: a state-of-the-art Monte Carlo code for research and development, Ann. Nucl. Energy 82 (2015) 90–97.
[28] B. Kouchunas, D. Jabaay, T. Downar, B.S. Collins, S.G. Stimpson, A.T. Godfrey, K.S. Kim, J.C. Gehin, S. Palmtag, F. Franceschini, Validation and Application of the 3D Neutron Transport MPACT within CASL VERA-CS, Oak Ridge National Lab (ORNL), Oak Ridge, TN (United States), 2015.
[29] R. Tuominen, V. Valtavirta, J. Leppänen, New energy deposition treatment in the Serpent 2 Monte Carlo transport code, Ann. Nucl. Energy 129 (2019) 224–232.
[30] OpenMC User's Guide, https://github.com/openmc-dev/openmc/blob/develop/docs/source/io_formats/settings.rst.
[31] M. Herman, A. Trkov, ENDF-6 Formats Manual, Brookhaven National Laboratory, 2009.
[32] The NJOY Nuclear Data Processing System, 2016. Version, https://github.com/njoy/NJOY2016-manual/raw/master/njoy16.pdf.
[33] G.F. Knoll, Radiation Detection and Measurement, John Wiley & Sons, 2010.
[34] S. Choi, D. Lee, Three-dimensional method of characteristics/diamond-difference transport analysis method in STREAM for whole-core neutron transport calculation, Comput. Phys. Commun. 260 (2021), 107332.
[35] J. Jang, W. Kim, S. Jeong, E. Jeong, J. Park, M. Lemaire, H. Lee, Y. Jo, P. Zhang, D. Lee, Validation of UNIST Monte Carlo code MCS for criticality safety analysis of PWR spent fuel pool and storage cask, Ann. Nucl. Energy 114 (2018) 495–509.
[36] J. Yu, H. Lee, H. Kim, P. Zhang, D. Lee, Simulations of BEAVRS benchmark cycle 2 depletion with MCS/CTF coupling system, Nucl. Eng. Technol. 52 (4) (2020) 661–673.

[37] H. Lee, E. Jeong, H. Lee, H.C. Lee, D. Lee, Verification of MCS VHTR modeling capability, in: Proceedings of the RPHA17 Conference, Chengdu: Nuclear Power Institute of China, August 24-25, 2017.
[38] M. Lemaire, H. Lee, B. Ebiwonjumi, C. Kong, W. Kim, Y. Jo, J. Park, D. Lee, Verification of photon transport capability of UNIST Monte Carlo code MCS, Comput. Phys. Commun. 231 (2018) 1–18.
[39] T. Goorley, M. James, T. Booth, F. Brown, J. Bull, L.J. Cox, J. Durkee, J. Elson, M. Fensin, R.A. Forster, J. Hendricks, Initial MCNP6 release overview, Nucl. Technol. 180 (3) (2012) 298–315.
[40] M. Lemaire, F. Setiawan, H. Lee, P. Zhang, D. Lee, Validation of coupled neutron-photon transport mode of Monte Carlo code MCS, in: Proceedings of the International Conference on Mathematics and Computational Methods Applied to Nuclear Science and Engineering M&C 2019, Portland, USA, August 25-29, 2019.
[41] M. Lemaire, H. Lee, P. Zhang, D. Lee, Interpretation of two SINBAD photon-leakage benchmarks with nuclear library ENDF/B-VIII. 0 and Monte Carlo code MCS, Nucl. Eng. Technol. 52 (7) (2020) 1355–1366.
[42] K.S. Kim, Specification for the VERA Depletion Benchmark Suite, Consortium for Advanced Simulation of LWRs, 2015. CASL-X-2015-1014-000.
[43] International Atomic Energy Agency, Database of Prompt Gamma Rays from Slow Neutron Capture for Elemental Analysis, IAEA, Vienna, 2007.
[44] K.D. Sevier, Atomic electron binding energies, Atomic Data Nucl. Data Tables 24 (4) (1979) 323–371.
[45] J. Rhodes, K. Smith, Z. Xu, CASMO-5 energy release per fission model, in: Proceedings of PHYSOR2008; Switzerland, 2008, pp. 14–19. September.
[46] W. Lee, S. Choi, B. Ebiwonjumi, M. Lemaire, D. Lee, Implementation of on-the-fly energy release per fission model in STREAM, in: Proceedings of the RPHA17 Conference, Chengdu: Nuclear Power Institute of China, August 24-25, 2017.
[47] Y. Liu, R. Salko, K.S. Kim, X. Wang, M. Kabelitz, S. Choi, B. Kochunas, B. Collins, W. Martin, Improved MPACT energy deposition and explicit heat generation coupling with CTF, Ann. Nucl. Energy 152 (2021), 107999.
[48] US Nuclear Regulatory Commission, Westinghouse Technology Systems Manual, 2011. Retrieved from, https://www.nrc.gov/docs/ML1122/ML11223A208.pdf.
[49] S. Kinast, D. Tomatis, Energy deposition in coolant of PWR under normal operation and accident conditions, Nucl. Eng. Des. 384 (2021), 111479.